

































literary and educational knowledge and information.”<sup>14</sup> Among other services, OCLC and its members are responsible for maintaining the WorldCat database,<sup>15</sup> used by independent and institutional libraries throughout the world.

37. OCLC also provides its members online access to MARC records through its OCLC bibliographic database. When an OCLC member institution acquires a work, it creates a MARC record for this work in its computer catalog system in the ordinary course of its business. MARC records created at the Library of Congress are directly uploaded or may be tape-loaded into the OCLC database through a subscription to MARC Distribution Services daily or weekly. Once the MARC record is created by a cataloger at an OCLC member institution or is tape-loaded from a participating institution, the MARC record is then made available to any other OCLC members online, and therefore made available to the public. Accordingly, once the MARC record is created by a cataloger at an OCLC member institution or is tape-loaded from the Library of Congress or another library anywhere in the world, any publication corresponding to the MARC record has been cataloged and indexed according to its subject matter such that a person interested in that subject matter could, with reasonable diligence, locate and access

---

<sup>14</sup> Third Article, Amended Articles of Incorporation of OCLC Online Computer Library Center, Inc., available at <https://www.oclc.org/content/dam/oclc/membership/articles-of-incorporation.pdf> (last accessed February 17, 2025).

<sup>15</sup> WorldCat, <http://www.worldcat.org/> (last accessed February 17, 2025).

































































































































hanksb  
spacing

world wide [PGH95, Rap96, Stü96]. Characteristic for systems of the first generation are the analog frequency modulation technique and the allocation of different non-overlapping frequency bands for individual connections. The separation of the user signals in the frequency domain is called frequency division multiple access (FDMA) [Pro95, Rap96, Stü96].

Parallel to the progress in wireless communications significant advances in digital communications took place. The origins of digital communications go back to the work of S. Morse in 1837, demonstrating an electrical telegraphy system. The so-called Morse code represents the letters of the alphabet by sequences of dots and dashes and was the precursor of modern variable-length source coding. The beginnings of modern digital communications stem from the work from H. Nyquist in 1924, who derived the maximum signaling rate that can be sent over a channel of a given bandwidth without intersymbol interference (ISI). Based on Nyquist's work, C.E. Shannon presented the fundamental limits of digital communication systems when he derived the channel capacity in 1948. The channel capacity determines the maximum information rate at which error free transmission is theoretically possible through the channel by appropriate coding. In the following years efficient digital signal processing techniques were developed such as source coding for data compression, encryption for security, and channel coding for error protection.

The rapid development in the area of micro electronics with a continuous increase in device density of integrated circuits and the development of low-rate digital speech coding techniques made completely digital second generation cellular mobile radio systems viable [PGH95]. Various second generation cellular systems were developed in the 1990s. Most of these systems employ time division multiple access (TDMA), such as the Global System for Mobile Communications (GSM) and the Digital Cellular System 1800 (DCS1800) in Europe, the Interim Standard (IS-) 54 in the USA, and the Personal Digital Cellular (PDC) system in Japan [PGH95, Rap96, Stü96]. With TDMA, the time axis is subdivided into different non-overlapping time slots where each user is exclusively assigned its time slots in which this user employs the total available bandwidth. Thus, TDMA separates the users in the time domain [Pro95, Rap96, Stü96]. In practice, TDMA is combined with FDMA to reduce the hardware complexity of an otherwise extremely broadband system and to increase the flexibility of the system.

Parallel to the TDMA based second generation standards, the IS-95 was developed in the USA, employing code division multiple access (CDMA) with direct sequence (DS) spectrum spreading, combined with FDMA [PGH95, Rap96, Vit95, Stü96]. The origins of CDMA go back to the beginnings of spread spectrum communications in the first half of the 20st century [Sch82]. Primary applications of spread spectrum communications lay in the development of secure digital communication systems for military use. Since the second half of the 20st century, spread spectrum communications became of great interest also for commercial applications, including mobile multi-user communications. Spread spectrum signals are characterized by their used bandwidth, which is much greater than the minimum necessary bandwidth for data transmission [Dix94, BGP84]. The spectrum spreading is achieved by using a spreading code that is

independent of the message and is known to the receiver. The receiver uses a synchronized replica of the spreading code to despread the received signal allowing recovery of the message. The large redundancy inherent in spread spectrum signals is required to overcome interference caused by the nature of the channel, by intentional disturbances, and by multiple access of various users. The exploitation of the spread spectrum technique to enable multiple users a simultaneous access to the channel is called CDMA. The separation of the user signals is performed in the code domain by applying user specific matched filtering in the receiver, referred to as despreading. Three principles of user specific spectrum spreading may be distinguished, namely DS, frequency hopped (FH), and time hopped (TH) spreading [Dix94, SOS94]. With FH spreading and TH spreading, the user specific spreading code is used to pseudo randomly hop the carrier frequency through a large bandwidth and to pseudo randomly hop the time slots through a large time duration, respectively. With DS spreading, the user specific spreading code introduces rapid phase transitions into the data stream, expanding the required bandwidth.

Wireless mobile communication systems of the 21st century have to ensure a wide range of multimedia services such as speech, image, and data transmission with different and variable bit rates up to 2 Mbit/s in hierarchical cell structures and in multi-operator scenarios [PGH95, BJK96]. The new services have to be available in indoor and outdoor environments, where the integration of satellite links shall enable world-wide coverage [PGH95, BJK96]. These requirements cannot be completely covered by the second generation systems, which have a relatively low available bit rate in the range of 10 kbit/s per user, primarily designed for speech transmission applications. Research activities concerning the standardization of the third generation mobile radio systems are in progress world-wide [PGH95, BJK96, Jun95]. International investigations run under the generic term Future Public Land Mobile Telecommunications Systems (FPLMTS) or also International Mobile Telecommunications 2000 (IMT-2000), and in Europe they are referred to as Universal Mobile Telecommunications Systems (UMTS) [PGH95, BJK96, Rap96]. An important challenge for UMTS and IMT-2000 is the selection of an appropriate multiple access scheme to meet the demands of third generation mobile radio systems. Within the program Research and Development in Advanced Communications Technologies in Europe, Phase II (RACE II), the two projects referred to as Code Division Testbed (CODIT) [BFG94] and advanced TDMA (ATDMA) [CDE94] can be mentioned as examples for a DS-CDMA and a TDMA concept, respectively, developed for UMTS. Both projects ran from 1992 till 1995 and their results were presented for standardization at the European Telecommunication Standards Institute (ETSI) and at the International Telecommunications Union (ITU).

The pros and cons of FDMA, TDMA, CDMA, or any combination thereof have to be considered carefully. They all perform the same under ideal transmission conditions assuming optimal design. However, under real transmission conditions encountered in mobile communications, the multiple access schemes can perform with significant differences. Essential for a decision is a comparison between CDMA and TDMA since FDMA is a quasi natural component of any multiple access scheme [Bai94]. A multitude of publications addressed to this comparison have shown that no definite winner emerges and further investigations of hybrid multiple ac-

cess schemes have to be carried out to exploit the advantages of the various access schemes [JBS93, Bai94, BJK96, Bai96, Kle96, Agh96]. Furthermore, attention has to be focused on recent developments in wireless communications, such as in the field of multi-carrier (MC) communications [Bin90], which can possibly improve the conventional multiple access schemes. In 1993, various concepts based on a combination of DS-CDMA and MC modulation were proposed [FaP93, YLF93, Van93, KoM93, Faz93, DaS93, CBJ93]. These novel CDMA concepts with MC modulation are described and discussed in the following section.

## 1.2 Multi-Carrier CDMA for Mobile Communications

### 1.2.1 Principles of DS Spread Spectrum and Multi-Carrier Modulation

Before introducing the new CDMA concepts based on MC modulation, a brief introduction to the basic elements DS spread spectrum and MC modulation is given in this section. A three-dimensional time/frequency/power density representation, shown in Fig. 1.1, is introduced to illustrate the principles of the various CDMA concepts and of MC modulation. A box indicates

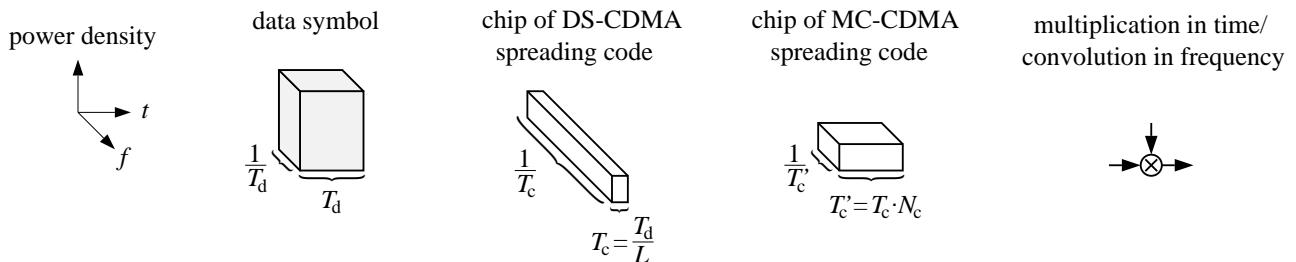


Figure 1.1: Three-dimensional time/frequency/power density representation

the three-dimensional time/frequency/power density range of the signal, in which most of the signal energy is located and does not make any statement about the pulse or spectrum shaping. The representation is normalized on the energy of a data symbol with duration  $T_d$  and rate  $1/T_d$ , respectively. For comparison, a chip of a DS-CDMA spreading code and of an MC-CDMA spreading code, explained in detail in the sequel, are shown.

The principle of DS spreading, comprehensively explained in [Dix94, BGP84, SOS94, Vit95, Pra96, Rap96], is illustrated in Fig. 1.2. The data symbols of a user are spectrally spread before transmission on carrier  $f_c$  by multiplying them with a user specific spreading code. The user specific DS-CDMA spreading code consists of  $L$  chips, each of duration  $T_c$ , cf. Fig. 1.1. The chip rate  $1/T_c$  is a factor  $L$  larger than the data symbol rate  $1/T_d$ . The factor  $L$  corresponds to the spreading code length and is also referred to as bandwidth spreading factor or processing gain. With DS-CDMA, multiple users simultaneously use the total available bandwidth at the same time, performing the separation of the user signals in the code domain.

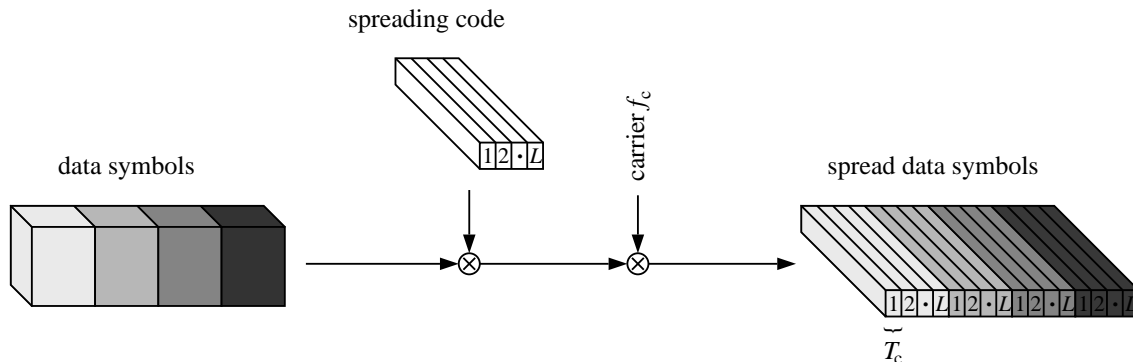


Figure 1.2: Principle of DS spreading of the data of a single user;  $T_c = T_d/L$

The progress in wireless communications entails a demand for higher data rates and, thus, shorter symbol durations. However, if the duration of the transmitted symbol becomes smaller than the time dispersion of the multipath channel, the performance of the wireless communication system suffers from ISI. This is a crucial problem since the receiver complexity is related to the amount of ISI. An approach to prevent ISI is offered by parallel data transmission [Cha66, Sal67, WeE71], referred to as MC communications. The principle of MC modulation, depicted in Fig. 1.3, is to convert a high rate data stream into  $N_c$  low-rate substreams, where  $N_c$  is the number of subcarriers used for data transmission. Each substream is modulated on its

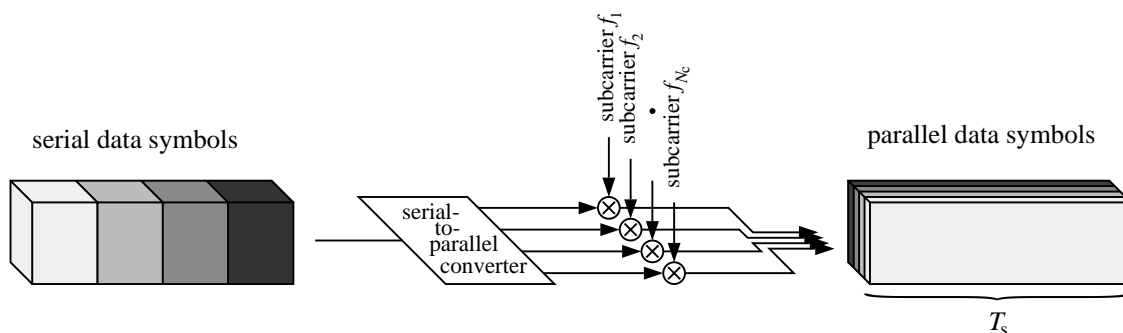


Figure 1.3: Principle of multi-carrier modulation;  $T_s = T_d N_c$

assigned subcarrier  $f_n$ ,  $n = 1, \dots, N_c$ . Thus, the available channel bandwidth is subdivided into  $N_c$  narrow subbands, which ideally appear frequency non-selective. The data symbol rate per subcarrier is reduced by a factor  $N_c$  and with that, the ISI is reduced. A common realization of MC communications is conventional frequency division multiplexing where the subbands are completely separated in the frequency domain. However, due to finite steepness of the filter roll-offs, the subchannel spacing has to be greater than the Nyquist bandwidth to avoid inter-subchannel interference (ICI). This inefficient use of the available spectrum can be overcome by permitting spectral overlap between adjacent subchannels [Cha66, Sal67]. ICI can be avoided by guaranteeing orthogonality between the signals on the subcarriers. With rectangular pulse shaping, orthogonality between the signals is obtained by choosing a subcarrier spacing equal to the reciprocal of the symbol duration per subcarrier  $T_s$ , known as orthogonal frequency division multiplexing (OFDM) [WeE71, Hir81, Cim85]. The  $N_c$  parallel modulated data symbols

of duration  $T_s$  equal to  $N_c \cdot T_d$  are referred to as an OFDM symbol with the assigned OFDM symbol rate  $1/T_s$ . By increasing the number of subcarriers, the OFDM spectrum approaches an ideal rectangular shaping within the bandwidth  $B$ .

The origins of MC communications go back to the 1950s as one of the earliest MC systems, the so-called Kineplex system with 20 subcarriers, each with a data rate of 150 bit/s, was presented [DHM57]. Since the amount of filters and oscillators is considerable for a larger number of subcarriers, an efficient digital implementation of OFDM was proposed by using the discrete Fourier transform (DFT) or its more computationally efficient implementation, the fast Fourier transform (FFT) [WeE71]. The progress in semiconductor technology enabled the realization of an FFT for a high number of subcarriers up to several thousands whereby OFDM gained much in significance. Residual ISI in MC communications can be avoided completely if a guard interval is added to each OFDM symbol, which has to be chosen larger than the time dispersion of the channel [All87, Bin90]. The breakthrough of MC communications came in the 1990s as OFDM was chosen for the European Digital Audio Broadcasting (DAB) standard [All87] and also for the European terrestrial Digital Video Broadcasting (DVB-T) standard [FKR95]. In broadcast applications, OFDM offers the possibility of operating in single frequency networks with a frequency reuse factor of one. The interference from neighbouring cells is experienced as artificial multipath reception causing additional ISI which can also be combatted by the guard interval [FKR96].

### 1.2.2 CDMA Concepts with Multi-Carrier Modulation

The success of MC modulation in broadcast applications motivated many researchers to investigate the suitability of MC modulation for wireless mobile communications. First multiple access systems with MC modulation were published in 1993 and were based on DS-CDMA [FaP93, YLF93, Van93, KoM93, Faz93, DaS93, CBJ93]. Two different concepts of combining DS-CDMA with MC modulation were introduced. Concept I is referred to as MC-CDMA, also known as OFDM-CDMA or MC-SSMA, and is the topic of this thesis. Concept II was proposed in two variants, the first one is referred to as MC-DS-CDMA, the second one as multi-tone (MT) CDMA. For both Concept I and Concept II, all users simultaneously share the available bandwidth where the separation of the users signals is carried out in the code domain comparable to DS-CDMA.

**Concept I:** MC-CDMA is based on a serial concatenation of DS spreading, cf. Fig. 1.2, and MC modulation, cf. Fig. 1.3, [FaP93, YLF93, CBJ93]. The high rate DS spread data stream is MC modulated in such a way, that the  $L$  chips of a spread data symbol are transmitted in parallel on different subcarriers. Thus, the assigned data symbol is simultaneously transmitted on  $L$  subcarriers. If the number of subcarriers  $N_c$  is equal to the spreading code length  $L$ , MC-CDMA requires the total bandwidth for the transmission of a single data symbol comparable to DS-CDMA. When choosing  $L$  smaller than  $N_c$  and introducing an appropriate frequency interleaving, the flexibility of an MC-CDMA system can be increased and the complexity of

the data detector can be reduced [FaP93, Faz93]. Fig. 1.4 shows the principle of an equivalent realization of the serial concatenation of DS spreading, cf. Fig. 1.2, and MC modulation, cf. Fig. 1.3. Each data symbol is copied onto  $L$  substreams before multiplication with one chip

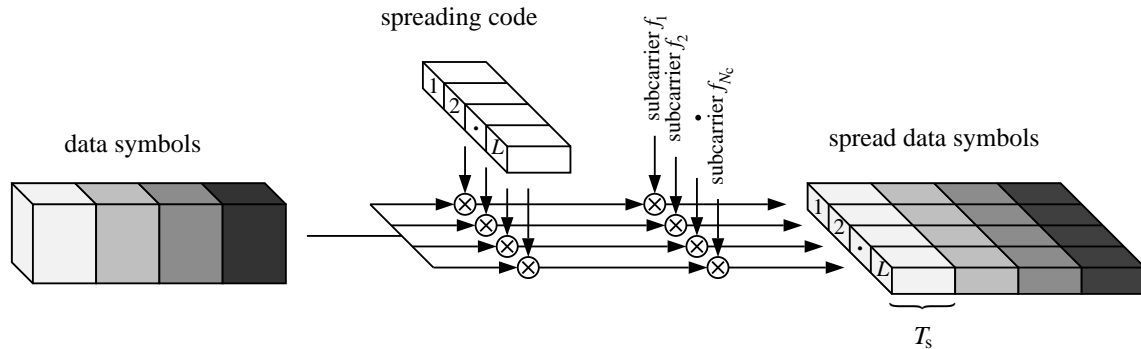


Figure 1.4: Principle of spreading of the data of a single user by MC-CDMA for the case  $N_c = L$ , i.e.,  $T_s = T_d$  and  $T'_c = T_d$

of the spreading code per substream. A chip of the MC-CDMA spreading code grouped in the frequency domain has the duration  $T'_c$ , cf. Fig. 1.1, which is by a factor of  $N_c$  greater than the duration  $T_c$  of a chip of the DS-CDMA spreading code. The case of  $N_c$  equal to  $L$  is illustrated in Fig. 1.4, yielding that the data symbol duration  $T_d$ , the chip duration  $T'_c$ , and the OFDM symbol duration  $T_s$  are identical. Fig. 1.4 reflects the fact that MC-CDMA has a spreading code grouped in the frequency domain. Comparing the spread data symbols of DS-CDMA, cf. Fig. 1.2, with those of MC-CDMA, cf. Fig. 1.4, it can be seen that MC-CDMA offers an additional flexibility in the frequency domain, which results in simple methods for signal reconstruction in the frequency domain. MC-CDMA was introduced with OFDM for optimum use of the available bandwidth [FaP93, YLF93, CBJ93]. Most MC-CDMA systems were proposed for the downlink from a base station (BS) to a mobile station (MS) where powerful mobile receivers with low complexity are required [FaP93, YLF93, CBJ93]. The time/frequency synchronism between the users in the downlink allows a simple realization of an efficient channel estimation required for coherent detection.

An approach to mitigate the effect of ISI in mobile radio environments without the exploitation of a guard interval implies more complex receivers with joint detection (JD), however, overcomes the loss in data rate due to the guard interval [JBP96a, JBP96b]. This approach was considered for the uplink from an MS to a BS where more complex receivers can be applied in the fixed BS. Since MC-CDMA can be implemented as DS-CDMA with a spreading code structure in the time domain [JBP96a, NaS96], this approach can employ JD techniques which have been primarily developed for DS-CDMA in the uplink [KIB93, KKB94, JuB95, Kle96].

**Concept II:** With Concept II, the serial data stream is first converted into parallel low-rate substreams before applying DS spreading on each substream, see Fig. 1.5 [DaS94, CSP95a, SoN96, Van95]. When setting the number of subcarriers  $N_c$  to one, Concept II becomes identical to DS-CDMA. Concept II was proposed in the two variants MC-DS-CDMA and MT-CDMA.

MC-DS-CDMA modulates the substreams on subcarriers with a spacing of the reciprocal of the chip duration to guarantee orthogonality between the signals of the substreams after DS spreading [DaS94, CSP95a, SoN96]. A chip of the MC-DS-CDMA spreading code has the same duration  $T'_c$  as a chip of the MC-CDMA spreading code, cf. Fig. 1.1. Comparable with MC-CDMA, the OFDM symbol duration  $T_s$  is equal to the chip duration  $T'_c$ . If the spreading code length  $L$  is equal to the number of subcarriers  $N_c$ , as illustrated in Fig. 1.5, or less than  $N_c$ , a single data symbol is not spread in bandwidth with MC-DS-CDMA, instead, it is extended in the time. The design of MC-DS-CDMA systems with a high number of subchannels, where

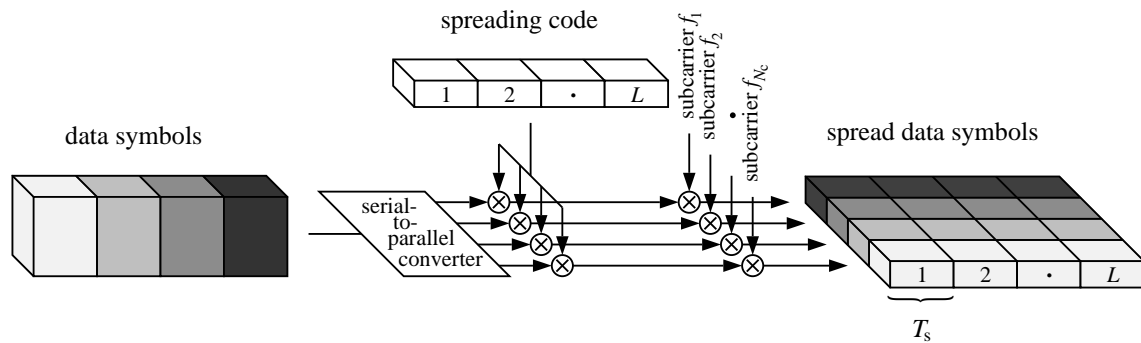


Figure 1.5: Principle of spreading of the data of a single user by MC-DS-CDMA for the case  $N_c = L$ , i.e.,  $T_s = T_d$  and  $T'_c = T_d$

each subchannel can be considered as frequency non-selective, is advantageous in the sense of exploiting time diversity. However, due to the frequency non-selective fading per subchannel, frequency diversity can only be exploited if channel coding with appropriate interleaving [CSP95a] or subcarrier hopping [CSP95b] is used, or if the same information is transmitted in parallel on several subcarriers [SoN96]. This could be extended to the case where the same information is transmitted on all subcarriers [KoM93, KoM96]. The latter approach implies a repetition coding, reducing the data rate by a factor of  $N_c$ . The MC-DS-CDMA system investigated in [KoM96] chooses a subcarrier spacing which is larger than the reciprocal of the chip duration with the intention to increase the frequency diversity of the system. The system considered in [KoM96] is primarily designed as a CDMA system overlaid onto existing narrow-band systems. MC-DS-CDMA uses  $N_c$  coherent non-RAKE receivers for data detection and was investigated for the quasi-synchronous and also for the asynchronous uplink.

MT-CDMA applies the same data mapping and spreading as MC-DS-CDMA. However, in contrast to MC-DS-CDMA, the subcarrier spacing is a factor of  $N_c$  smaller than the reciprocal of the chip duration [Van93, Van95]. Thus, the  $N_c$  parallel converted data symbols before DS spreading fulfill the orthogonality requirements [Van93, Van95]. The DS spreading per subcarrier violates the orthogonality requirements, hence, introducing ICI. However, tight subcarrier spacing enables the use of spreading codes which are longer by a factor of approximately  $N_c$  compared to the spreading codes of DS-CDMA, assuming the same total available bandwidth. Therefore, the system may be able to supply more users than with DS-CDMA at the expense

of ICI [HaP96]. Since each subchannel is affected by frequency selective fading in a multipath channel, a RAKE receiver or more complex multi-user detectors can be applied per subchannel as investigated in [Van93, Van95, Van97] and therein included references. MT-CDMA was investigated for the asynchronous uplink.

A multitude of research activities was addressed to performance comparisons between MC-CDMA, DS-CDMA, MC-DS-CDMA, and MT-CDMA [CBJ93, Kai95a, HLP95, Kai95b, FKS95, HaP96, PrH96, JBP96b, Pra96]. The bit error rate (BER)  $P_b$  and the bandwidth efficiency  $\beta$  of a mobile radio system with perfect channel estimation and without channel coding were chosen as decision criterion. The bandwidth efficiency is defined as [Pra96]

$$\beta = \frac{K_{\text{sys}} R_b}{B}, \quad (1.1)$$

where  $K_{\text{sys}}$  is the user capacity of the mobile radio system in a single cell,  $R_b$  is the bit rate per user, and  $B$  is the total used bandwidth. The user capacity  $K_{\text{sys}}$  is the maximum possible number of simultaneously active users at a certain signal-to-noise ratio (SNR) for which the BER is less or equal to a predefined threshold. The bandwidth efficiency is a measure for the maximum achievable bit rate at a given bandwidth of an isolated cell with the dimension bit/s/Hz [Pra96]. The bandwidth efficiency has to be distinguished from the cellular spectrum efficiency [BKN94, Ste96]. The cellular spectrum efficiency is a measure for the maximum achievable bit rate at a given bandwidth per cell while maintaining a required service quality within a cellular system and has the dimension bit/s/Hz/cell [BKN94, Ste96].

First comparisons were carried out between MC-CDMA and DS-CDMA with RAKE receiver, applied in the downlink of a mobile radio system [Kai95a, HLP95, Kai95b, FKS95]. It was demonstrated that MC-CDMA can outperform DS-CDMA with RAKE receiver significantly with respect to the BER for a high number of active users and can achieve an about four times higher bandwidth efficiency  $\beta$ . Advantageous for MC-CDMA is the application of orthogonal spreading codes by guaranteeing optimal code synchronization in the receiver due to the spreading code structure in the frequency domain. Furthermore, the absence of ISI enables an efficient utilization of the total received energy for signal detection with low complexity. Other performance comparisons for the downlink include MC-DS-CDMA and MT-CDMA and confirm that only MC-CDMA, but not MC-DS-CDMA and MT-CDMA, can significantly outperform DS-CDMA with a RAKE receiver [HaP96, PrH96]. MC-DS-CDMA and MT-CDMA systems provide results similar to those obtained with DS-CDMA. Moreover, a BER performance comparison between MC-CDMA with JD and DS-CDMA with JD for the uplink shows a slightly better performance with MC-CDMA [JBP96b].

Finally, a performance comparison of MC-CDMA with the recently proposed MC-FDMA and MC-TDMA [ReR94, RoG96a, RoG96b, HaP96, Kai96] reveals in the uncoded and the coded case of a downlink mobile radio system advantages for MC-CDMA [Kai96]. Since the performance of MC-FDMA and MC-TDMA is used as a reference throughout the thesis, both multiple access schemes will be briefly introduced.

The combination of FDMA and TDMA, respectively, with MC modulation employing OFDM is referred to as MC-FDMA and MC-TDMA, respectively, in the sequel. Other references also use the names OFDM-FDMA and OFDM-TDMA. In an MC-FDMA system, the data symbols for different users are transmitted on different subcarriers. One or several subcarriers are exclusively allocated to a user for transmission [ReR94, HaP96, Kai96]. An advantage of MC-FDMA compared to conventional FDMA is that with OFDM an optimal bandwidth utilization of the available bandwidth is guaranteed without ICI. However, the performance of an uncoded MC-FDMA system is poor in a mobile radio channel since the frequency non-selectivity per subchannel causes dominant performance degradations if a subcarrier is located in a deep fade. Channel coding is necessary for MC-FDMA systems to enable the exploitation of diversity. In the case of MC-TDMA, the whole bandwidth is allocated to a single user for a certain number of OFDM symbols [RoG96a, RoG96b, Kai96]. The complexity of conventional TDMA systems is determined by the amount of ISI caused by the mobile radio channel. In MC-TDMA systems, the long OFDM symbol duration drastically can reduce the amount of ISI which can completely be avoided by the used of a guard interval. MC-TDMA needs channel coding in the same way as MC-FDMA to enable the exploitation of diversity.

### 1.2.3 State of the Art in the Field of MC-CDMA

The employment of MC-CDMA for mobile multi-user communications has become an active field of research since 1993. Up to now, the majority of publications in the field of MC-CDMA was devoted to the investigation of data detection techniques suitable for mobile radio systems in the downlink. Due to the novelty of the subject, investigations including the potential of channel coding with code bit interleaving or the influence of non-perfect channel estimation were scarcely carried out. This section gives an overview on the state of the art concerning the topics data detection, channel coding, and channel estimation applied in MC-CDMA mobile radio systems. Contributions to these topics made by the author of the thesis are not included in this overview. These contributions will be presented in the Chapters 3 to 6.

Important contributions to the field of MC-CDMA data detection techniques are summarized in Table 1.1 and can be classified as either single-user detection (SD) or multi-user detection (MD). The conventional approach with SD detects the user signal of interest by not taking into account any information about the multiple access interference (MAI). In MC-CDMA mobile radio systems, SD is realized by one tap equalization to compensate for the distortion due to flat fading on each subcarrier, followed by user specific despreading [Faz93, YLF93, CBJ93]. The one tap equalizer is simply one complex-valued multiplication per subcarrier. Under ideal transmission conditions, SD performs optimally in MC-CDMA mobile radio systems, since synchronous transmission with orthogonal spreading codes is applied. However, in non-ideal channels with frequency selective fading due to multipath propagation, the orthogonality between the signals of the different users is lost and MAI occurs. A multitude of SD techniques was proposed to combat the channel fading and, thus, the MAI, cf. Table 1.1. Basic SD techniques investigated and evaluated for MC-CDMA mobile radio systems are equal gain combining

Table 1.1: Contributions to the field of data detection for MC-CDMA mobile radio systems

classification	references	detection technique
SD	[Faz93][YLF93]	EGC
	[Faz93][CBJ93]	ZF equalization
	[YLF93][DeK97]	MRC
	[CBJ93][YeL94b]	MMSE equalization
	[FBA94]	RAKE in the frequency domain
	[YeL94a][RoB96]	controlled equalization
	[NaS96]	EGC, MRC, ZF equalization, and MMSE equalization in the time domain
	[NaF97]	RAKE in the time domain
MD	[Faz93][HLP95] [KaP96b][MaO97a] [StP97b]	IC
	[FaP93][Faz93]	JD with MLSE
	[JBP96b]	JD with ZF equalization and MMSE equalization, both with and without decision feedback
	[TER97]	JD with recurrent neural network structure

(EGC) [Faz93, YLF93], zero-forcing (ZF) equalization [Faz93, CBJ93], maximum ratio combining (MRC) [YLF93], and minimum mean square error (MMSE) equalization [CBJ93]. Further SD techniques are classified in Table 1.1.

As long as the spreading code structure of the interfering signals is known, the MAI is not noise-like, yielding SD to be suboptimal. The suboptimality of SD can be overcome with MD where the a priori knowledge about the spreading codes of the interfering users is exploited in the detection process [Kle96, Pro95]. The performance improvements with MD compared to SD are achieved at the expense of higher receiver complexity. The methods of MD can be divided into interference cancellation (IC) and JD [Kle96]. The principle of IC is to detect the information of the interfering users with SD and to reconstruct the interfering contribution in the received signal before subtracting, i.e., cancelling the interfering contribution from the received signal and detecting the information of the desired user. The iterative application of IC leads to a multistage detection scheme [VaA90]. IC can be carried out parallel for all interfering users when the amount of interference from each user is similar, first investigated for MC-CDMA mobile radio systems in [Faz93]. Another method of IC would be successive IC where per iteration the contribution of the strongest interferer remaining after the previous IC stage is cancelled. Successive IC is especially well suited in the case of users, interfering with different signal strength. The optimal detector applies JD with maximum likelihood

sequence estimation (MLSE) or maximum likelihood symbol-by-symbol estimation (MLSSE), respectively [Pro95]. Since the complexity of MLSE and of MLSSE grows exponentially with the number of users, their use is limited in practice to applications with a small number of users. By applying a hybrid MC-CDMA system with an integrated FDMA structure on subcarrier level, this requirement can be fulfilled and JD can be realizable in MC-CDMA mobile radio systems with low complexity [FaP93]. Further JD techniques are classified in Table 1.1.

MC modulated systems with flat fading per subchannel require either the use of spread spectrum techniques or of channel coding to exploit diversity. Interleaving further improves the diversity gain achievable with both approaches. MC systems with channel coding such as DAB and DVB-T systems [All87, FKR95] and coded MC-FDMA and coded MC-TDMA mobile radio systems [Kai96] yield promising results. Channel coding also considerably improves the performance of MC-CDMA systems which already exploit diversity due to the spread spectrum technique [FaP93, JBB97]. Binary convolutional codes were chosen as channel codes in the MC-CDMA mobile radio systems [FaP93, StP97a]. Investigations of MC-CDMA mobile radio systems with channel coding are summarized in Table 1.2. The combination of spreading and

Table 1.2: Contributions to the field of channel coding for MC-CDMA mobile radio systems

references	coding technique & <i>comments</i>
[FaP93][MaO97a] [StP97a][StP97b] [JBB97]	convolutional coding
[MaO96][StP97a]	low rate orthogonal convolutional coding; <i>used for spreading also</i>

channel coding by applying a low-rate orthogonal convolutional code [Vit90] for both spreading and coding in MC-CDMA systems [MaO96, StP97a] show that this approach achieves only a low bandwidth efficiency [StP97a].

Coherent data detection as well as channel decoding exploiting reliability information require knowledge about the channel and, thus, channel estimation. MC systems with OFDM allow channel estimation by exploiting the correlation of the fading process in frequency and time. Pilot symbol aided channel estimation realized by a two-dimensional filter or two one-dimensional filters working sequentially [Höh91] is a promising concept for MC-CDMA receivers operating in mobile radio environments [MBR96]. Various principles of channel estimation concepts proposed for the down- and the uplink of MC-CDMA mobile radio systems are summarized in Table 1.3.

Finally, the suitability of MC-CDMA systems was, for instance, investigated for cellular mobile radio applications in [TCC97, JBB97] and for wireless local area networks in [CFR96, BCF96].

The overview of research activities in the field of data detection, channel coding, and channel estimation for MC-CDMA mobile radio systems in Tables 1.1 to 1.3 reflects that a multitude of

Table 1.3: Contributions to the field of channel estimation for MC-CDMA mobile radio systems

link	references	principle of channel estimation & <i>comments</i>
downlink	[CFG95]	reference OFDM symbols; <i>indoor</i>
	[MRG95]	pilot symbols with filtering in two dimensions
	[ToK96c]	least-squares algorithm with training symbols; <i>indoor</i>
uplink	[CFG95]	reference OFDM symbols; <i>indoor</i>
	[Ste97a][Ste97b]	pilot tones
	[JBB97][BJP97]	single-carrier modulated midamble

research activities were carried out in the last years. However, the overview also demonstrates that, especially when looking at the beginning of the research for this thesis in 1994, many problems were open and are still open, which form the motivation for this thesis presented in the following section.

### 1.3 Goals of the Thesis

Proceeding from the state of the art and from emerging, still uncovered fields, the thesis has two main objectives. The first objective is to find and optimize appropriate concepts for the single components data detection, channel decoding, and channel estimation applied in MC-CDMA mobile radio systems. The second objective is to analyze the performance of a complete MC-CDMA mobile radio system in various mobile radio environments in the downlink. To reach these objectives, in particular, the following goals are pursued:

- CDMA concepts with MC modulation known from literature shall be put together and shall be classified. This has already been accomplished in Section 1.2.2.
- The MC-CDMA signal structure shall be mathematically described. By introducing appropriate modifications, the flexibility of MC-CDMA mobile radio systems shall be pointed out. Techniques for SD and MD applied in MC-CDMA mobile radio systems shall be developed, evaluated, and as far as possible, analyzed theoretically. A comparative overview of the performance of novel and known SD and MD techniques for MC-CDMA mobile radio systems shall be given.
- Table 1.2 shows that MC-CDMA mobile radio systems with channel coding and code bit interleaving were rarely investigated. MC-CDMA systems have to be considered with various channel coding schemes applying hard and soft decision decoding. Furthermore, recent developments in the field of iterative channel decoding have to be taken into account. Since decoders based on the Viterbi algorithm should exploit log-likelihood ratios (LLRs) as soft inputs with optimum reliability information, the LLRs for coded

MC-CDMA systems with soft decision decoding applying SD as well as MD have to be derived. The iterative concatenation of data detection and decoding for IC with reliability information shall be investigated. The trade-off between coding and spreading in MC-CDMA mobile radio systems shall be found.

- A powerful channel estimation concept is required for MC-CDMA systems to guarantee efficient coherent data detection and soft decision channel decoding. Channel estimation concepts with filtering in two dimensions shall be developed and analyzed generally for MC modulated systems operating in mobile radio channels with fast time variation and large time dispersion, typical for large cells.
- Future cellular mobile radio systems have to operate in hierarchical cell structures with cells of various size, adapted to the specific environment and requirement. Three typical cell classifications can be distinguished, macro-, micro-, and picocells, where each class has its characteristic signal propagation. To the best of the author's knowledge, no complete system analysis of a coded MC-CDMA mobile radio system with non-perfect channel estimation for all three propagation scenarios typical for future cellular concepts is available. An extensive system analysis of an MC-CDMA system in the downlink with channel coding and non-perfect channel estimation shall be carried out for mobile radio channels, typical for macro-, micro-, and picocell propagation scenarios. This analysis shall prove the suitability of an MC-CDMA system as a potential candidate for future mobile radio systems.

## 1.4 Contents and Important Results

The thesis consists of 7 chapters, where the contents of the Chapters 3 to 6 correspond to the goals mentioned in Section 1.3.

The fundamentals of time variant multipath propagation, which characterize the demands on a mobile radio system, are summarized in Chapter 2. After describing the mobile radio channel and its statistical modelling, channel models typical for future cellular mobile radio systems are classified for macro-, micro-, and picocells.

In Chapter 3, the MC-CDMA concept under investigation is presented. After an introduction into MC modulation with OFDM, the MC-CDMA signal structure is explained and its flexibility is pointed out by introducing the  $M$ -, the  $Q$ -, and the  $M&Q$ -Modification. A discrete-time and -frequency MC-CDMA transmission model is mathematically described using the vector-matrix notation. Low-complex SD techniques, a multistage detection technique with IC, where the detection stages are adapted to the residual MAI, and the optimum JD with MLSSE are developed and analyzed for MC-CDMA systems. Their performance is demonstrated and compared to known SD and MD techniques based on Monte Carlo simulations. The principle of MC-FDMA and MC-TDMA is briefly introduced and the performance of MC-CDMA, MC-FDMA, and MC-TDMA systems is compared to each other. Finally, the equivalence between MC-CDMA and DS-CDMA is pointed out in Chapter 3.

The adaptation of channel coding with soft decision decoding and code bit interleaving to MC-CDMA systems is treated in Chapter 4. Convolutional encoding with conventional and different iterative decoding strategies employing the Viterbi algorithm are investigated. To guarantee an optimum concatenation of data detection and soft decision channel decoding, the optimum soft decided values which can be delivered to a Viterbi decoder, are derived for MC-CDMA receivers with SD and with MD. Exploiting the optimum soft decided values, an iterative detection and decoding scheme referred to as soft IC is introduced. With soft IC, reliability information about the reconstructed interference is taken into account in the iterative IC scheme, reducing error propagation. An important result is that IC based on soft decided values from the channel decoder significantly outperforms JD with MLSSE followed by soft decision channel decoding. In Chapter 4, also the suitability of the recently proposed Turbo codes as channel codes for MC-CDMA systems is investigated. However, it is shown that Turbo codes are only of limited use in MC-CDMA systems when considering speech transmission applications. Iterative Turbo decoding outperforms simpler conventional Viterbi decoding only when applying large Turbo code interleaver sizes, resulting in large delays which are not permitted in speech transmission applications. The trade-off between spreading and coding in MC-CDMA systems is determined and a bandwidth efficiency plan for MC-CDMA, MC-FDMA, and MC-TDMA systems is presented. It can be concluded that the performance of coded MC-CDMA systems with SD and MD, respectively, applying code rates  $R$  less than  $2/3$  improves with spreading codes of increasing length up to  $L$  equal to 8. A further increase of the spreading code length results in no relevant performance gain.

In Chapter 5, a pilot symbol aided channel estimation for MC systems with filtering of the fading process in time and frequency is analyzed and optimized. Model mismatch between the correlation functions of the channel and those used for the filter design is taken into account in the analysis. An appropriate arrangement of the pilot symbols in an OFDM frame based on the two-dimensional sampling theorem is presented, where the redundancy due to pilot symbols is less than 6%. It is shown that the performance of the presented low-complex channel estimation with two one-dimensional FIR filters working sequentially closely approximates the performance of a channel estimation with an optimum two-dimensional Wiener filter.

A complete MC-CDMA system is designed and analyzed in the downlink of a mobile radio system in Chapter 6. The system evaluation takes into account channel coding, non-perfect channel estimation, and propagation scenarios typical for macro, micro, and picocells. The suitability of the developed MC-CDMA system for mobile radio environments with high Doppler frequencies of 400Hz and with large time dispersion of  $20 \mu s$  is demonstrated. Guaranteeing a good transmission quality with a coded BER  $P_b$  equal to  $10^{-3}$ , the presented MC-CDMA mobile radio system achieves the remarkable bandwidth efficiency of 0.81 bit/s/Hz at an SNR per bit between 8 dB and 12 dB on the average.

Chapter 7 contains an abstract and a German summary of the thesis.

# Chapter 2

## Mobile Radio Channel

### 2.1 Time-Variant Multipath Propagation

Splitting the service area of a mobile radio system into multiple geographically separated cells enables the reuse of the same frequency band in different cells. Besides the frequency reuse which considerably increases the number of simultaneously communicating users within the service area, cell splitting reduces the required transmission power with decreasing cell size. Within a cell, a BS serves a number of roaming MSs. The cells in mobile radio communications vary substantially in size and shape and are, for instance, adapted to areas with low density fast moving vehicular MSs and areas with high density low speed portable MSs. Three typical cell classifications can be distinguished [COD95, FIL96]:

- **Macrocells** have a radius of 1 km to 35 km. The basic categories of macrocells are urban, suburban, rural, and hilly environments. The BS antenna is elevated well above the local terrain. Rarely a direct line of sight (LOS) path between the BS and the MS antennas exists because of the natural and man-made objects that are in immediate vicinity of the MS. Due to the large size of macrocells, they are suited for the support of MSs with high velocities due to the lower handoff rate compared to smaller cells.
- **Microcells** typically have a radius of 20 m to 300 m and are found in urban areas and city centers. The determining characteristic is that the BS antenna height is under the mean level of the surrounding roof tops. In microcells, LOS is the situation often found. Microcells with a radius up to 1 km have the BS antenna situated above the mean surrounding roof tops. The velocity of the MSs is mainly the speed of pedestrians and city traffic.
- **Picocells** have a radius up to 100 m and are typically applicable to indoor like environments. LOS between the BS and the MS antenna is mostly present if both antennas are inside the same room. The velocity of the MSs in picocells is typically on the order of a few km/h.

The link between a BS and an MS is given by the mobile radio channel. In the mobile radio channel, the transmitted signal suffers from three nearly independent effects which are characterized as follows:

- **Multipath propagation** occurs as a consequence of reflections, scattering, and diffraction of the transmitted electromagnetic wave at natural and man-made objects. Thus, at the receiver antenna, a multitude of waves arrives from many different directions with different delays, attenuations, and phases. The superposition of the waves results in amplitude and phase variations of the composite received wave. Due to the mobility of the MS and moving objects in the mobile radio channel, changes in the phases and amplitudes of the arriving waves occur, resulting in time-variant multipath propagation. Even small movements on the order of the wavelength may result in a totally different wave superposition. The varying signal strength due to time-variant multipath propagation is referred to as fast fading.
- **Shadowing** is caused by obstruction of the transmitted waves by hills, buildings, walls, etc., resulting in more or less strong attenuation of the signal strength. Compared to fast fading, longer distances have to be covered to significantly change the shadowing constellation. The varying signal strength due to shadowing is called slow fading and can be described by a log-normal distribution [Par92].
- **Path loss** predicts how the mean signal power decays with distance from the BS. In free space, the mean signal power decreases with the square of the distance from the BS. In a mobile radio channel, where often no direct LOS path exists between the BS and the MS antennas, the signal power typically decreases with a power higher than two and is typically in the order of three to five [Rap96].

Variations of the received power due to shadowing and path loss can be counteracted by power control and are not considered further in this thesis. In this section, the mobile radio channel is described with respect to its fast fading characteristic. A statistical description of the multipath channel is chosen [Bel63], since a deterministic description appears impossible in practice. Throughout the thesis, all bandpass signals and channels are replaced by equivalent lowpass signals and channels for mathematical convenience but with no loss of generality [Pro95, Rup93]. The lowpass representation is in general complex-valued. In the sequel, complex values are marked by underlining. The symbol  $(.)^*$  denotes the complex conjugation.

The mobile radio channel is given by the time-variant channel impulse response  $\underline{h}(\tau, t)$  or by the time-variant channel transfer function  $\underline{H}(f, t)$ , which is the Fourier transform of  $\underline{h}(\tau, t)$ . The channel impulse response represents the response of the channel at time  $t$  due to an impulse applied at time  $t - \tau$ . The mobile radio channel is assumed as a wide-sense stationary (WSS) random process, i.e., the channel has a fading statistic that remains constant over short periods of time or small spatial distances. In environments with multipath propagation, the channel impulse response is composed of a large number of scattered impulses received over  $N_p$  different paths,

$$\underline{h}(\tau, t) = \sum_{p=1}^{N_p} a_p e^{j(2\pi f_{D,p} t + \varphi_p)} \delta(\tau - \tau_p), \quad (2.1)$$

where  $a_p$ ,  $f_{D,p}$ ,  $\varphi_p$ , and  $\tau_p$  are the amplitude, the Doppler frequency, the phase, and the propagation delay, respectively, associated with the  $p$ th path. The Doppler frequency

$$f_{D,p} = \frac{v f_c}{c} \cos \alpha_p \quad (2.2)$$

depends on the velocity  $v$  of the MS, the speed of light  $c$ , the carrier frequency  $f_c$ , and the angle of incidence  $\alpha_p$  of a wave assigned to the  $p$ th path.

The description of the correlation functions of the channel impulse response  $\underline{h}(\tau, t)$  is sufficient to characterize the fast fading of the mobile radio channel [Bel63]. The autocorrelation function of  $\underline{h}(\tau, t)$  is defined as

$$\underline{R}(\tau_1, \tau_2, \Delta t) = \frac{1}{2} \text{E}\{\underline{h}(\tau_1, t) \underline{h}^*(\tau_2, t + \Delta t)\}. \quad (2.3)$$

Under the presumption that the WSS random processes  $\underline{h}(\tau_1, t)$  and  $\underline{h}(\tau_2, t)$  are uncorrelated for  $\tau_1$  not equal to  $\tau_2$ , called uncorrelated scattering (US), the autocorrelation function (2.3) simplifies to

$$\underline{R}(\tau_1, \tau_2, \Delta t) = \underline{\rho}(\tau_1, \Delta t) \delta(\tau_1 - \tau_2), \quad (2.4)$$

where  $\underline{\rho}(\tau, \Delta t)$  is the delay cross-power spectral density [Bel63]. The mobile radio channel characterized by (2.4) is referred to as WSSUS channel. The Fourier transform of  $\underline{\rho}(\tau, \Delta t)$  in  $\Delta t$  yields the scattering function [Bel63]

$$S(\tau, f_D) = \int_{-\infty}^{\infty} \underline{\rho}(\tau, \Delta t) e^{-j2\pi f_D \Delta t} d(\Delta t). \quad (2.5)$$

The scattering function is real-valued and provides a measure of the average power output of the channel as a function of the delay  $\tau$  and the Doppler frequency  $f_D$ .

By integrating the scattering function  $S(\tau, f_D)$  over the Doppler frequency  $f_D$ , the delay power density spectrum

$$\rho(\tau) = \int_{-\infty}^{\infty} S(\tau, f_D) df_D, \quad (2.6)$$

is obtained, which is identical to the delay cross-power spectral density  $\underline{\rho}(\tau, \Delta t)$  at  $\Delta t$  equal to 0. The delay power density spectrum gives the average power of the channel output as a function of the delay  $\tau$  and can be viewed as a scattering function averaged over all Doppler shifts. The mean delay  $\bar{\tau}$ , the delay spread  $\sigma_\tau$ , and the maximum delay  $\tau_{\max}$  are characteristic parameters of a multipath channel and can be determined from the delay power density spectrum. If the duration  $T_s$  of the transmitted symbol is significantly larger than the maximum delay  $\tau_{\max}$ , the channel produces a negligible amount of ISI. This effect is exploited with MC transmission where the duration per transmitted symbol increases with the number of subcarriers and, hence, the amount of ISI decreases. Residual ISI can be eliminated by the use of a guard interval, cf. Section 1.2.1. The time dispersive properties of multipath channels are most commonly

quantified by their mean delay and the delay spread [Par92]. The mean delay is the first moment of the delay power density spectrum resulting in

$$\bar{\tau} = \frac{\int_0^{\infty} \tau \rho(\tau) d\tau}{\int_0^{\infty} \rho(\tau) d\tau}. \quad (2.7)$$

The normalization with  $\int_0^{\infty} \rho(\tau) d\tau$  is applied because  $\rho(\tau)$  is not a probability density function. The delays are measured relative to the first detectable path at the receiver. The delay spread is the standard deviation of the delay power density spectrum and is given by

$$\sigma_{\tau} = \sqrt{\frac{\int_0^{\infty} (\tau - \bar{\tau})^2 \rho(\tau) d\tau}{\int_0^{\infty} \rho(\tau) d\tau}}. \quad (2.8)$$

The coherence bandwidth  $(\Delta f)_c$  of a mobile radio channel is the bandwidth over which the signal propagation characteristics are correlated and is proportional to the reciprocal of the delay spread  $\sigma_{\tau}$ . The coherence bandwidth can be defined as the bandwidth over which the frequency correlation function is above 0.5 and, thus, can be approximated by [Rap96, Skl97a]

$$(\Delta f)_c \approx \frac{1}{5\sigma_{\tau}}. \quad (2.9)$$

The frequency correlation function is the Fourier transform of the delay power density spectrum  $\rho(\tau)$ , i.e.,

$$\underline{\theta}(\Delta f) = \int_{-\infty}^{\infty} \rho(\tau) e^{-j2\pi\tau\Delta f} d\tau. \quad (2.10)$$

The channel is said to be frequency selective if the signal bandwidth  $B$  is larger than the coherence bandwidth  $(\Delta f)_c$ . On the other hand, if  $B$  is smaller than  $(\Delta f)_c$ , the channel is said to be frequency non-selective or flat. The coherence bandwidth of the channel is of importance for evaluating the performance of spreading and frequency interleaving techniques that try to exploit the inherent frequency diversity  $D_f$  of the mobile radio channel. In the case of MC transmission, frequency diversity is exploited if the separation of subcarriers transmitting the same information exceeds the coherence bandwidth. The maximum achievable frequency diversity is approximated by the ratio between the signal bandwidth  $B$  and the coherence bandwidth  $(\Delta f)_c$ ,

$$D_f \approx \frac{B}{(\Delta f)_c}, \quad (2.11)$$

and, consequently, depends on the delay spread  $\sigma_{\tau}$  of the channel, cf. (2.9).

By integrating the scattering function  $S(\tau, f_D)$  over the delay  $\tau$ , the Doppler power density spectrum

$$S_{f_D}(f_D) = \int_{-\infty}^{\infty} S(\tau, f_D) d\tau \quad (2.12)$$

is obtained. The Doppler power density spectrum gives the average power of the channel output as a function of the Doppler frequency  $f_D$  and can be viewed as a scattering function averaged over all delays. The frequency dispersive properties of multipath channels are most commonly quantified by the maximum occurring Doppler frequency  $f_{D_{\max}}$ . If in the case of MC transmission the subchannel spacing is significantly larger than the maximum Doppler frequency  $f_{D_{\max}}$ , the channel produces a negligible amount of ICI. The coherence time of the channel  $(\Delta t)_c$  is the duration over which the channel characteristics can be considered as time-invariant and is proportional to the reciprocal of the maximum Doppler frequency. The coherence time can be defined as the time over which the time correlation function is above 0.5 and, thus, can be approximated by [Ste94, Rap96]

$$(\Delta t)_c \approx \frac{9}{16\pi f_{D_{\max}}}. \quad (2.13)$$

The time correlation function is the inverse Fourier transform of the Doppler power density spectrum  $S_{f_D}(f_D)$ , i.e.,

$$\varrho(\Delta t) = \int_{-\infty}^{\infty} S_{f_D}(f_D) e^{j2\pi f_D \Delta t} df_D. \quad (2.14)$$

If the duration  $T_s$  of the transmitted symbol is larger than the coherence time  $(\Delta t)_c$ , the channel is said to be time selective. On the other hand, if  $T_s$  is smaller than  $(\Delta t)_c$ , the channel is said to be time non-selective. The coherence time of the channel is of importance for evaluating the performance of coding and interleaving techniques that try to exploit the inherent time diversity  $D_t$  of the mobile radio channel. Time diversity can be exploited if the separation between successive time slots carrying the same information exceeds the coherence time. A number of  $N_s$  successive time slots create a time frame of duration  $T_{fr}$ . The maximum time diversity achievable in one time frame is approximated by the ratio between the duration  $T_{fr}$  of a time frame and the coherence time  $(\Delta t)_c$ ,

$$D_t \approx \frac{T_{fr}}{(\Delta t)_c}, \quad (2.15)$$

which, consequently, depends on the maximum Doppler frequency  $f_{D_{\max}}$  of the channel, cf. (2.13).

A system exploiting frequency and time diversity can achieve the overall diversity

$$D = D_f \cdot D_t. \quad (2.16)$$

The system design should allow one to optimally exploit the available diversity  $D$ . For instance, in systems with MC transmission the same information should be transmitted on different subcarriers and in different time slots, achieving uncorrelated fading in both dimensions. In MC systems, a time slot corresponds to an OFDM symbol. Further diversity schemes like space, angle, or polarization diversity which are not within the scope of this thesis can additionally increase the overall diversity and are described in [Jak74, Lee93, Rap96, Stü96]. It should be noted that space diversity, also known as antenna diversity, is a popular form of diversity used in wireless systems [BBS97].

Several probability distributions can be considered in attempting to model the statistical characteristics of the fading process. A simple and often used approach is obtained from the assumption that there is a large number of scatterers in the channel that contribute to the signal at the receiver. The application of the central limit theorem leads to a complex-valued Gaussian process for the channel impulse response. In the absence of a LOS or a dominant component, the process is zero-mean. The magnitude of the corresponding channel transfer function

$$a(f, t) = |\underline{H}(f, t)| \quad (2.17)$$

is a random variable, for brevity denoted by  $a$ , with a Rayleigh distribution given by [Pro95]

$$p(a) = \frac{2a}{\Omega} e^{-a^2/\Omega}, \quad a \geq 0, \quad (2.18)$$

where

$$\Omega = E\{|\underline{H}(f, t)|^2\} \quad (2.19)$$

is the average power. The phase is uniformly distributed in the interval  $[0, 2\pi[$ . This channel is said to be a Rayleigh fading channel and best agrees with the propagation characteristic of macrocells.

In the case that the multipath channel contains a LOS or dominant component in addition to the randomly moving scatterers, the channel impulse response can no longer be modeled as zero-mean. Under the assumption of a complex-valued Gaussian process for the channel impulse response, the magnitude of the channel transfer function has a Rice distribution given by [Pro95]

$$p(a) = \frac{2a(K_{\text{Rice}} + 1)}{\Omega} e^{-K_{\text{Rice}} - a^2(K_{\text{Rice}} + 1)/\Omega} I_0\left(2a\sqrt{\frac{K_{\text{Rice}}(K_{\text{Rice}} + 1)}{\Omega}}\right), \quad a \geq 0. \quad (2.20)$$

The Rice factor  $K_{\text{Rice}}$  is determined by the ratio of the power of the dominant path to the power of the scattered paths at the receiver. The average power  $\Omega$  is given according to (2.19) and  $I_0(\cdot)$  is the zero-order modified Bessel function of first kind. The phase is uniformly distributed in the interval  $[0, 2\pi[$ . This channel is said to be a Ricean fading channel and best agrees with the propagation characteristic of micro- and picocells.

An alternative, more empirical approach to statistically model the magnitude  $|\underline{H}(f, t)|$  distribution of the channel transfer function, by providing a closer match to some experimental data than either the Rayleigh or Rice distribution, is given by the Nakagami- $m$  distribution, introduced by Nakagami in the early 1940's [Nak60]. The Nakagami- $m$  distribution describes the magnitude  $|\underline{H}(f, t)|$  distribution by a central chi-square distribution with  $m$ , not necessarily integer, degrees of freedom and is defined as [Nak60, Stü96]

$$p(a) = \frac{2a^{2m-1}}{\Gamma(m)} \left(\frac{m}{\Omega}\right)^m e^{-ma^2/\Omega}, \quad a \geq 0, \quad (2.21)$$

where

$$m = \frac{\Omega^2}{E\{(a^2 - \Omega)^2\}}, \quad m \geq \frac{1}{2}. \quad (2.22)$$

The average power  $\Omega$  over all paths is given according to (2.19) and  $\Gamma(\cdot)$  is the Gamma function. The parameter  $m$  is related to the fading strength and can be used to model fading conditions that are more or less severe than those modelled according to the Rayleigh distribution. In the case of a dominant path, the Nakagami- $m$  distribution can closely approximate the Rice distribution by using the following relations between the Rice factor  $K_{\text{Rice}}$  and the Nakagami parameter  $m$  [Nak60, Stü96],

$$K_{\text{Rice}} = \frac{\sqrt{m^2 - m}}{m - \sqrt{m^2 - m}}, \quad m \geq 1, \quad (2.23)$$

and

$$m = \frac{(K_{\text{Rice}} + 1)^2}{(2K_{\text{Rice}} + 1)}. \quad (2.24)$$

A statistical description of the fading process based on the Nakagami- $m$  distribution often leads to closed analytical expressions, while the Rice distribution due to the Bessel function does not. If  $m$  and, thus,  $K_{\text{Rice}}$  approach infinity, the Nakagami- $m$  distribution and the Rice distribution become an impulse, corresponding to an ideal channel. If  $m$  is equal to 1 and, thus,  $K_{\text{Rice}}$  is equal to 0, the Nakagami- $m$  distribution and the Rice distribution become a Rayleigh distribution. If  $m$  is in the interval  $[1/2, 1[$ , the fading conditions become more severe than Rayleigh fading and the distribution reduces for  $m$  equal to 1/2 to a one-sided Gaussian distribution. Thus, the Nakagami- $m$  distribution is the most flexible of the three presented distributions. Moreover, the simple algebraic form of  $m$  and  $\Omega$  allows a straightforward extraction of these parameters from measured data [BrD91], as applied for the definition of macro-, micro-, and picocell propagation models in the CODIT study [COD95]. The channel models defined in the CODIT study are described in the following section.

## 2.2 Channel Models for Macro-, Micro-, and Picocells

### 2.2.1 CODIT and COST 207 Channel Models

The investigations of the MC-CDMA mobile radio system proposed in this thesis should be carried out on a basis which takes into account the requirements of future mobile radio systems. Thus, different channel models typical for macro-, micro-, and picocells are required. The channel models of two different studies are chosen for the investigations in this thesis. Namely, the propagation models of the CODIT study [COD95, FIL96], defined for macro-, micro-, and picocell scenarios, and the propagation models of the COST 207 study [COS89, FIL96], defined for macrocell scenarios only. Throughout the thesis, these two types of channel models are referred to as CODIT channel models and COST 207 channel models. The use of both types of channel models for the investigations should, besides the evaluation of the MC-CDMA system, enable a comparison between the CODIT and the COST 207 channel models. Furthermore, performance comparisons with other mobile radio systems which take into account any of these

channel models should be enabled. In the following, the different philosophies behind the CODIT and the COST 207 channel models are pointed out and the implementation of the channel models of both studies is described.

The philosophy of modelling the mobile radio channel with the CODIT and COST 207 approach is related to the physical description of the channel and is based on the implementation of a discrete multipath scenario. This type of channel modelling enables the reconstruction of a scattering function  $S(\tau, f_D)$  obtained from measured mobile radio channels. The channel impulse response corresponds to (2.1), where the  $N_p$  discrete paths may differ in the amplitudes, Doppler frequencies, phases, and propagation delays. The assigned channel transfer function becomes

$$\underline{H}(f, t) = \sum_{p=1}^{N_p} a_p e^{j(2\pi f_{D,p} t + \varphi_p)} e^{-j2\pi f \tau_p} \quad (2.25)$$

and is chosen for the implementation of the CODIT and COST 207 channel models in this thesis, since channels with MC transmission can be simulated computationally efficiently in the frequency domain. Preconditions for the frequency domain implementation are the absence of ISI and ICI, the frequency non-selective fading per subcarrier, and the time-invariance during one OFDM symbol. The investigated MC-CDMA mobile radio systems are designed to fulfill these preconditions. Thus, a discrete representation of the channel transfer function is enabled according to

$$\underline{H}_{n,i} = \underline{H}(nF_s, iT'_s) = \sum_{p=1}^{N_p} a_p e^{j(2\pi f_{D,p} iT'_s + \varphi_p)} e^{-j2\pi nF_s \tau_p}, \quad (2.26)$$

where  $\underline{H}(f, t)$  is sampled in time at OFDM symbol rate  $1/T'_s$  and in frequency at subcarrier spacing  $F_s$ . The OFDM symbol duration  $T'_s$  includes the guard interval duration. The basic differences between the CODIT channel models and the COST 207 channel models originate in the defined amplitude, Doppler frequency, and propagation delay distributions.

The **CODIT channel models** describe the fading characteristics of the various propagation environments by the parameters of the Nakagami- $m$  distribution. Every environment is defined in terms of a number of scatterers which can take on values up to 20. The number of scatterers is equal to the number of paths  $N_p$ . Each scatterer  $p$ ,  $p = 1, \dots, N_p$ , is characterized by a path delay  $\tau_p$ , an angle of incidence  $\alpha_p$ , a Nakagami parameter  $m_p$ , and an average power  $\Omega_p$ . The approach of the CODIT channel models is based on a wave interference problem and assumes that the signal strength produced by one scatterer is caused by the sum of a sufficiently large number of waves, superimposed at the receiver. Each scatterer is composed of a number of  $N_w$  waves which is equal to 100, and, if existent, of one dominant component. The spatial scatterer model used in the CODIT channel models is illustrated in Fig. 2.1. The spatial scatterer model is applied for macro-, micro-, and picocell scenarios. The propagation delay  $\tau_p$  and the average power  $\Omega_p$  of the  $p$ th scatterer are taken from a uniform distribution within the interval  $[\tau_{p,\min}, \tau_{p,\max}]$  and  $[\Omega_{p,\min}, \Omega_{p,\max}]$ , respectively, independently for each scatterer. The channel is

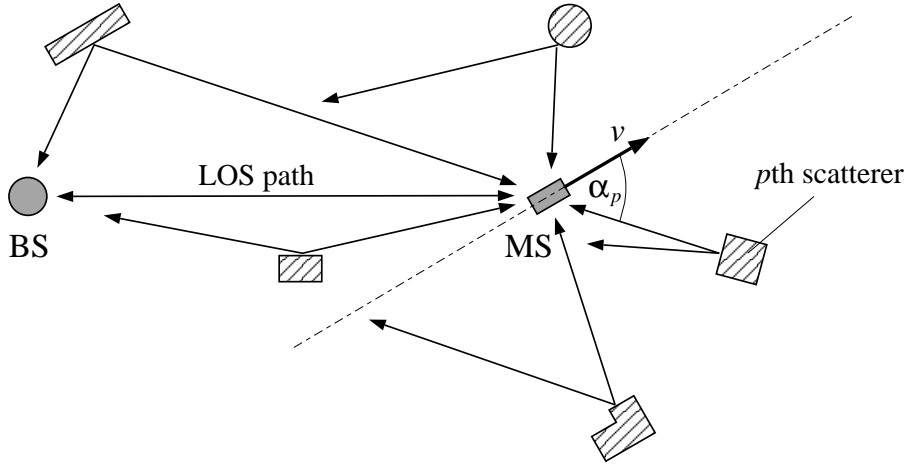


Figure 2.1: Spatial scatterer model used in the CODIT channel models

power normalized, so that

$$\Omega = \sum_{p=1}^{N_p} \Omega_p = 1. \quad (2.27)$$

The Nakagami parameter  $m_p$  of each scatterer  $p$ ,  $p = 1, \dots, N_p$ , is explicitly indicated, except for one channel model where an interval of a uniform distribution is defined. In the sequel, the joint index  $p, w$  indicates a variable assigned to the  $w$ th wave of the  $p$ th scatterer, with  $p = 1, \dots, N_p$  and  $w = 1, \dots, N_w$ . The index  $p, 0$  indicates a variable assigned to the, if existent, dominant component of the  $p$ th path. The wave amplitudes  $a_{p,w}$ ,  $p = 1, \dots, N_p$ ,  $w = 1, \dots, N_w$ , are obtained from a zero-mean Gaussian distribution with variance

$$\sigma_{a_{p,w}}^2 = \frac{\Omega_p}{N_w} \left( 1 - \sqrt{1 - \frac{1}{m_p}} \right), \quad p = 1, \dots, N_p, \quad w = 1, \dots, N_w. \quad (2.28)$$

If a dominant component exists, its amplitude  $a_{p,0}$  is given by

$$a_{p,0} = \sqrt{\Omega_p \sqrt{1 - \frac{1}{m_p}}}, \quad p = 1, \dots, N_p. \quad (2.29)$$

The Doppler power density spectrum is defined by the spatial scatterer distribution and the mobile velocity according to (2.2). The angle of incidence  $\alpha_p$  per scatterer is taken from a uniform distribution within the interval  $[\alpha_{p,\min}, \alpha_{p,\max}]$  or is predefined by the location of other scatterers assuming correlation between these scatterers. Correlation between the angles of incidence is given in propagation scenarios like in streets or corridors where the signal propagation is concentrated in a certain direction. Thus, the  $N_p$  angles of incidence of the scatterers are not necessarily uniformly distributed within the whole interval  $[0, 2\pi[$ . However, if an isotropic distribution of the scatterers is chosen, a classical Doppler power density spectrum according to Clarke is obtained [Par92]. The angle of incidence of the, if existent, dominant component  $\alpha_{p,0}$  is equal to  $\alpha_p$  and the angles of the waves  $\alpha_{p,w}$ ,  $w = 1, \dots, N_w$ , are obtained from a Gaussian distribution with standard deviation of 0.15 radians and mean  $\alpha_p$ . Each wave has a phase  $\varphi_{p,w}$ ,

Table 2.1: CODIT channel model parameters; each scatterer is composed of  $N_w = 100$  waves and, if existent, one dominant component; the angle of incidence per wave is taken from a Gaussian distribution with mean  $\alpha_p$  and standard deviation of 0.15 radians; values between brackets  $[a, b]$  mean that the value is taken from a uniform distribution within  $a$  and  $b$

cell type	environment	$N_p$	$p$	$\Omega'_p$	$m_p$	$\alpha_p$	$\tau_p$ in $\mu s$
macro	suburban (SU)	6	1	1	15	$[0, 2\pi]$	0
			2-6	$[0.1, 0.4]$	$[1, 5]$	$[0, 2\pi]$	$[0.1, 15]$
	urban (U)	20	1-20	$[0.5, 1.5]$	1	$[0, 2\pi]$	$[0, 2]$
	rural (R)	1	1	1	25	$[0, 2\pi]$	0
micro	urban 1 (Mic1)	20	1	1	3	$[0, 2\pi]$	0
			2-20	$[0.1, 0.4]$	1	$[0, 2\pi]$	$[0, 1]$
	urban 2 (Mic2)	20	1-20	$[0.5, 1.5]$	1	$[0, 2\pi]$	$[0, 1]$
pico	indoor 1 (Pic1)	12	1	1	8	$\alpha_0 \in [0, 2\pi]$	0
			2-7	$[0.03, 0.5]$	4	$\alpha_0 \pm [0, \pi/3]$	$[0.01, 0.05]$
			8-12	$[0.001, 0.03]$	1	$[0, 2\pi]$	$[0.025, 0.125]$
	indoor 2 (Pic2)	20	1	1	3	$[0, 2\pi]$	0
			2-10	$[0.1, 1]$	2	$[0, 2\pi]$	$[0.01, 0.1]$
			11-20	$[0.001, 0.1]$	1	$[0, 2\pi]$	$[0.1, 0.5]$

$w = 0, \dots, N_w$ , chosen randomly within the interval  $[0, 2\pi[$ , so that the superposition of the waves corresponds to a random phase interference situation.

The channel transfer function implemented by the CODIT channel models can be written as

$$H_{n,i} = \sum_{p=1}^{N_p} \left( a_{p,0} e^{j(2\pi \frac{vfc}{c} iT'_s \cos(\alpha_{p,0}) + \varphi_{p,0})} + \sum_{w=1}^{N_w} a_{p,w} e^{j(2\pi \frac{vfc}{c} iT'_s \cos(\alpha_{p,w}) + \varphi_{p,w})} \right) e^{-j2\pi n F_s \tau_p}. \quad (2.30)$$

Table 2.1 shows the basic macro-, micro-, and picocell environments defined in the CODIT study and used for the investigations in this thesis. Further propagation scenarios for specific micro- and picocell scenarios are given in [COD95]. It has to be mentioned that the power of the scatterers  $\Omega'_p$  defined in Table 2.1 is not normalized according to (2.27). Therefore, the power of each scatterer has to be normalized by

$$\Omega_p = \frac{\Omega'_p}{\sum_{p=1}^{N_p} \Omega'_p}, \quad p = 1, \dots, N_p. \quad (2.31)$$

Exemplary, a scattering function  $S(\tau, f_D)$  typical for the urban environment defined in the CODIT study is plotted in Fig. 2.2. Each impulse train of the scattering function represents

the contribution of one scatterer of the total of 20 scatterers and consists of 100 waves, where the angles of incidence of the waves are Gaussian distributed around the mean  $\alpha_p$  of the assigned scatterer. The angles of incidence of the scatterers in the urban environment are uniformly distributed in the interval  $[0, 2\pi[$ , resulting in a classical Doppler power density spectrum according to Clarke [Par92].

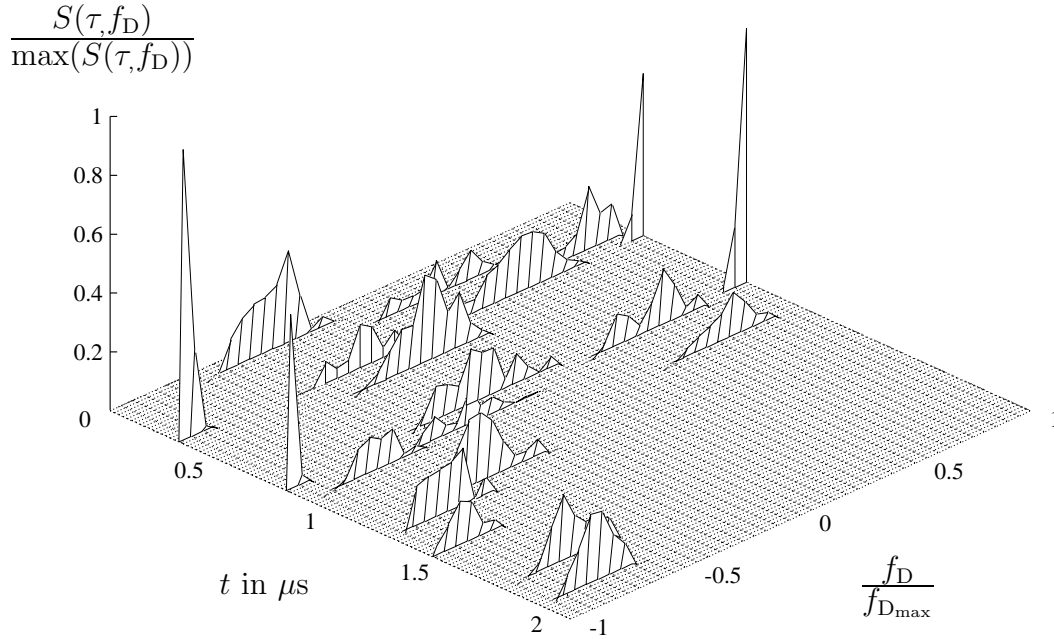


Figure 2.2: Scattering function of the urban environment defined in the CODIT study

The **COST 207 channel models** basically determine the various propagation scenarios by continuous, exponentially decreasing delay power density spectra  $\rho(\tau)$ . Every environment can be modeled by a number of  $N_p$  discrete paths, where each path has the same amplitude and is specified by its propagation delay  $\tau_p$  [Sch89]. Each propagation delay is chosen according to the probability density function of  $\tau$  within the given interval  $[\tau_{p,\min}, \tau_{p,\max}]$ . The probability density function of  $\tau$  is proportional to the delay power density spectrum  $\rho(\tau)$  [Höh92]. The average power  $\Omega_p$  per path is chosen to be  $1/N_p$ , normalizing the power of the channel according to (2.27). The  $N_p$  paths are modelled with isotropic scattering, i.e., the angles of incidence  $\alpha_p$  are taken from a uniform distribution in the interval  $[0, 2\pi[$ . Hence, a classical Doppler power density spectrum according to Clarke is obtained [Par92]. Each path has a phase  $\varphi_p$  uniformly distributed over the interval  $[0, 2\pi[$ .

The channel transfer function implemented by the COST 207 channel models can be written as

$$H_{n,i} = \frac{1}{\sqrt{N_p}} \sum_{p=1}^{N_p} e^{j(2\pi \frac{v f_c}{c} i T'_s \cos(\alpha_p) + \varphi_p)} e^{-j2\pi n F_s \tau_p}. \quad (2.32)$$

Table 2.2: COST 207 channel model parameters; the power per path is normalized to  $\Omega_p = 1/N_p$ ; the angles of incidence  $\alpha_p$  are taken from a uniform distribution in the interval  $[0, 2\pi[$ ; the propagation delays  $\tau_p$  are chosen within the given interval  $[\tau_{p,\min}, \tau_{p,\max}]$  proportional to the assigned delay power density function  $\rho(\tau)$

cell type	environment	$N_p$	$p$	$\Omega_p$	$m_p$	$\alpha_p$	$\tau_p$ in $\mu\text{s}$	$\rho(\tau)$
macro	hilly terrain (HT)	100	1-74	0.01	1	$[0, 2\pi]$	$[0, 2]$	$\propto e^{-3.5\tau_p/\mu\text{s}}$
			75-100	0.01	1	$[0, 2\pi]$	$[15, 20]$	$\propto 0.1 e^{15-\tau_p/\mu\text{s}}$
	bad urban (BU)	100	1-68	0.01	1	$[0, 2\pi]$	$[0, 5]$	$\propto e^{-\tau_p/\mu\text{s}}$
			69-100	0.01	1	$[0, 2\pi]$	$[5, 10]$	$\propto 0.5 e^{5-\tau_p/\mu\text{s}}$
typical urban (TU)	100	1-100	0.01	1	$[0, 2\pi]$	$[0, 7]$	$\propto e^{-\tau_p/\mu\text{s}}$	
rural area (RA)	100	1-100	0.01	1	$[0, 2\pi]$	$[0, 0.7]$	$\propto e^{-9.2\tau_p/\mu\text{s}}$	

Table 2.2 shows the macrocell environments defined in the COST 207 study, which are used for the investigations within this thesis. As mentioned before, the propagation environments defined within the COST 207 study are only valid for macrocell environments, and are not suitable for investigations with smaller cells, typical for future cellular systems.

When comparing the CODIT and the COST 207 channel models, the following statements can be made:

- The CODIT channel models are more flexible compared to the COST 207 channel models due to higher degrees of freedom given by the definition of the parameters  $\Omega_p$ ,  $m_p$ ,  $\alpha_p$ , and  $\tau_p$  individually for each path  $p$ ,  $p = 1, \dots, N_p$ . This enables one to implement a scattering function  $S(\tau, f_D)$  of a mobile radio channel which well approximates a measured scattering function.
- Compared to the COST 207 channel models, only the CODIT channel models define propagation scenarios for micro- and picocells which are especially of interest for the analysis of future mobile radio systems.
- Higher implementation efforts and simulation times have to be taken into account when using the CODIT channel models as opposed to the simple COST 207 channel models. This is the price to pay for increased flexibility and modelling accuracy.
- The COST 207 channel models are more popular than the CODIT channel models and, thus, more often enable comparisons to existing systems evaluated with the popular COST 207 channel models.

Generally, the CODIT channel models seems to be of higher relevance for investigations related closely to the propagation situations in real life and are of main interest in the MC-CDMA mobile radio system evaluation presented in Chapter 6. However, since the COST 207 channel models are more popular than the CODIT channel models, performance results of the MC-CDMA system with the COST 207 channel models are included also in Chapter 6. In the sequel, the propagation scenarios are referred to by the abbreviations given in brackets in Tables 2.1 and 2.2.

A comparison between the different CODIT and COST 207 channel models with respect to the mean delay, the delay spread, and the coherence bandwidth is presented in Table 2.3. The

Table 2.3: Characteristic values for the CODIT and COST 207 channel models

channel model	cell type	environment	$\bar{\tau}$ in $\mu\text{s}$	$\sigma_{\tau}$ in $\mu\text{s}$	$(\Delta f)_c$ in kHz
CODIT	macro	suburban (SU)	4.17	4.70	42.6
		urban (U)	1.00	0.58	344.8
		rural (R)	0	0	$\infty$
	micro	urban 1 (Mic1)	0.39	0.32	625.0
		urban 2 (Mic2)	0.50	0.29	689.7
	pico	indoor 1 (Pic1)	0.02	0.02	10000.0
indoor 2 (Pic2)		0.06	0.07	2857.1	
COST 207	macro	hilly terrain (HT)	4.36	6.90	29.0
		bad urban (BU)	2.62	2.52	79.4
		typical urban (TU)	0.99	0.98	204.1
		rural area (RA)	0.11	0.11	1818.2

coherence bandwidth  $(\Delta f)_c$  is obtained according to (2.9). The achievable frequency diversity  $D_f$  can be approximated with (2.11). It has to be mentioned that the COST 207 channel model HT offers less frequency diversity as obtained with (2.11), since the delay power density spectrum is non-zero only on a fraction of the interval  $[0, \tau_{\max}]$ . Hence, the achievable frequency diversity is approximately reduced by the ratio of the time over which the delay power density spectrum is non-zero to the maximum delay.

The time variability of mobile radio channels depends on the velocity  $v$  of the MSs. Each cell type has its typically occurring velocities of the MSs. Table 2.4 gives an overview on the velocities of the MS used in this thesis for the different cell types. Additionally, the Doppler frequency occurring at a carrier frequency of  $f_c$  equal to 1.8 GHz and the assigned coherence time according to (2.13) is given.

Table 2.4: Velocities of the MS, chosen for the different cell types; a choice is indicated by the symbol X

$v$ in km/h	$f_{D_{\max}}$ in Hz		cell type		
	$f_c = 1.8$ GHz	$(\Delta t)_c$ in ms $f_c = 1.8$ GHz	macro	micro	pico
3	5.0	35.8	X	X	X
30	50.0	3.6	X	X	-
150	250.0	0.7	X	-	-
250	416.7	0.4	X	-	-

### 2.2.2 Uncorrelated Fading Channel Model for Multi-Carrier Systems

The main disadvantage of channel models which are based on the implementation of a discrete multipath scenarios like the CODIT or COST 207 channel models are in general the high simulation times, because for each data symbol the contribution of each of the  $N_p$  paths must be calculated. When simulating broadband MC systems, this disadvantage can be overcome by fulfilling the following conditions:

- The MC system is provided with a frequency interleaver which guarantees that neighbouring symbols in the data stream fade independently, i.e., the interleaving depth exceeds the coherence bandwidth.
- An appropriate time interleaver, e.g., code bit interleaver, ensures that the fading in adjacent OFDM symbols can be modelled as independent.
- Frequency non-selective fading per subcarrier and time-invariance during one OFDM symbol have to be guaranteed, i.e., the subchannel bandwidth has to be smaller than the coherence bandwidth  $(\Delta f)_c$  and the symbol duration has to be smaller than the coherence time  $(\Delta t)_c$ .
- The absence of ISI and ICI has to be guaranteed by the use of a guard interval equal to or longer than the maximum delay of the channel  $\tau_{\max}$ .

These conditions enable one to model the fading channel computationally efficiently in the frequency domain. A symbol transmitted on the  $n$ th subchannel of the  $i$ th OFDM symbol is multiplied by a fading amplitude  $a_{n,i}$  chosen from a distribution  $p(a)$  according to the considered cell type, cf. Section 2.1, and a random phase  $\varphi_{n,i}$ , uniformly distributed over the interval  $[0, 2\pi[$ . The resulting complex-valued channel fading coefficient

$$\underline{H}_{n,i} = a_{n,i} e^{j\varphi_{n,i}} \quad (2.33)$$

is thus generated independently for each subcarrier and OFDM symbol. For a propagation scenario in a macrocell without LOS, the fading amplitude is generated by a Rayleigh distribution and the channel model is referred to as an uncorrelated Rayleigh fading channel. Analogously, for smaller cells where often a dominant propagation component occurs, the fading amplitude is chosen from a Rice distribution or Nakagami- $m$  distribution. The advantages of the uncorrelated fading channel model are the simple implementation, which can be observed when comparing (2.33) with (2.32) and (2.30), the computationally efficient system simulation, and the simple reproduction of the simulation results. These advantages are the reason for the often use of the uncorrelated fading channel models for the evaluation of MC modulated systems in multipath channels.

For the evaluation of MC-CDMA data detection techniques presented in Chapter 3 and the channel encoding and decoding strategies investigated in Chapter 4, the uncorrelated Rayleigh fading channel model is used with the intention of presenting the results as reference curves for further investigations. For the design of a channel estimation with filtering in time and frequency direction in Chapter 5 and its application in the complete MC-CDMA system evaluation in Chapter 6, the CODIT and COST 207 channel models are used, since correlated fading in time and frequency is required. Furthermore, the performance degradation due to a finite interleaver size can be shown with correlated fading.

# Chapter 3

## Multiple Access Scheme MC-CDMA

### 3.1 Multi-Carrier Communications

#### 3.1.1 Orthogonal Frequency Division Multiplexing

The principle of MC modulation is to map a serial high rate source stream onto multiple parallel low rate substreams and to modulate each substream on another subcarrier. Since the symbol rate on each subcarrier is much less than the serial source symbol rate, the effects of delay spread significantly decrease, reducing the complexity of the equalizer. OFDM is a low-complex technique to bandwidth-efficiently modulate multiple subcarriers by using the digital signal processing as introduced in Section 1.2.1. In the sequel, MC modulation based on OFDM is described and forms the basis for the introduction of the MC-CDMA signal structure in Section 3.2. One of the main design goals for an MC transmission scheme based on OFDM in a mobile radio channel is that the channel can be considered as time-invariant during one OFDM symbol and that the fading per subcarrier can be considered as flat. Thus, the OFDM symbol duration should be smaller than the coherence time  $(\Delta t)_c$  of the channel, cf. (2.13), and the subcarrier spacing should be smaller than the coherence bandwidth  $(\Delta f)_c$  of the channel, cf. (2.9). By fulfilling these conditions, the realization of low-complex receivers is possible.

A communication system with MC modulation transmits a sequence  $\{\underline{S}_n\}$  consisting of  $N_c$  complex-valued source symbols  $\underline{S}_n$ ,  $n = 1, \dots, N_c$ , in parallel on  $N_c$  subcarriers. Throughout the thesis, variables which can be interpreted as values in the frequency domain like the source symbols  $\underline{S}_n$ ,  $n = 1, \dots, N_c$ , each modulating another subcarrier frequency, are written with capital letters. The source symbols may, for instance, be obtained after source and channel coding, interleaving, and symbol mapping. For brevity, but without loss of generality, the transmission of a single but arbitrary sequence  $\{\underline{S}_n\}$  is considered in this chapter, so that no additional time index is required. The isolated consideration of  $\{\underline{S}_n\}$  is valid since ISI and ICI can be avoided with OFDM.

The MC modulator maps a sequence  $\{\underline{S}_n\}$  of  $N_c$  serial source symbols of rate  $1/T$  onto  $N_c$  parallel substreams, cf. Fig. 1.3. The source symbol rate per substream reduces to

$$\frac{1}{T_s} = \frac{1}{N_c T}. \quad (3.1)$$

According to OFDM, the  $N_c$  substreams are modulated on subcarriers with a spacing of

$$F_s = \frac{1}{T_s} \quad (3.2)$$

to achieve orthogonality between the signals on the  $N_c$  subcarriers, presuming a rectangular pulse shaping. The  $N_c$  parallel modulated source symbols  $S_n$ ,  $n = 1, \dots, N_c$ , are referred to as an OFDM symbol of duration  $T_s$ . The complex envelope of an OFDM symbol with rectangular pulse shaping has the form

$$\underline{x}(t) = \frac{1}{\sqrt{N_c}} \sum_{n=1}^{N_c} S_n \operatorname{rect}\left(\frac{t}{T_s} - \frac{1}{2}\right) e^{j2\pi f_n t}. \quad (3.3)$$

In (3.3), the factor  $1/\sqrt{N_c}$  normalizes the energy. The  $N_c$  subcarrier frequencies are located at

$$f_n = \frac{n-1}{T_s}, \quad n = 1, \dots, N_c, \quad (3.4)$$

where the center of the frequency spectrum is located at  $(N_c - 1)/(2T_s)$ . This definition of  $f_n$ ,  $n = 1, \dots, N_c$ , facilitates a simple mathematical modelling. The carrier frequency  $f_c$  determining the location of the signal in the bandpass domain is neglected in (3.4), since the equivalent lowpass domain is considered. The energy density spectrum  $|\underline{X}(f)|^2$  of an OFDM symbol is the sum of the energy density spectra of  $N_c$  independently modulated subcarriers and results in

$$|\underline{X}(f)|^2 = \frac{1}{N_c} \sum_{n=1}^{N_c} \left| S_n T_s \frac{\sin(\pi(f - f_n)T_s)}{\pi(f - f_n)T_s} \right|^2. \quad (3.5)$$

The normalized energy density spectrum of an OFDM symbol with  $N_c$  equal to 16 subcarriers versus the normalized frequency  $fT$  is depicted as a solid curve in Fig. 3.1. The OFDM spectrum is shown for the case where the symbols  $S_n$ ,  $n = 1, \dots, N_c$ , are transmitted with equal energy. The dotted curve illustrates the energy density spectrum of the first modulated subcarrier  $f_1$  and indicates the construction of the overall energy density spectrum as the sum of  $N_c$ , each by  $1/T_s$  shifted, individual energy density spectra. For large values of  $N_c$ , the energy density spectrum becomes more flat in the normalized frequency range of  $fT \in [-0.5, 0.5]$  containing the subcarriers. Only subcarriers near the band edges contribute to the out-of-band power. Therefore, as  $N_c$  becomes large, the energy density spectrum approaches that of single carrier modulation with ideal Nyquist filtering. As a reference, the normalized energy density spectrum of binary phase shift keying (BPSK) [Pro95] is plotted as a dashed curve.

A key advantage of using OFDM is that the MC modulation can be implemented in the discrete domain by using an IDFT, or a more computationally efficient IFFT [WeE71]. When sampling the complex envelope  $\underline{x}(t)$  of an OFDM symbol at time instances  $t$  equal to  $(\nu - 1)T_s/N_c$ ,  $\nu = 1, \dots, N_c$ , the samples are

$$\underline{x}_\nu = \frac{1}{\sqrt{N_c}} \sum_{n=1}^{N_c} S_n e^{j2\pi(n-1)(\nu-1)/N_c}, \quad \nu = 1, \dots, N_c, \quad (3.6)$$

and the sampling rate is  $N_c/T_s$ . The important result is that the sampled sequence  $\{\underline{x}_\nu\}$ ,  $\nu = 1, \dots, N_c$ , is the IDFT of the source symbol sequence  $\{S_n\}$ ,  $n = 1, \dots, N_c$ . The block

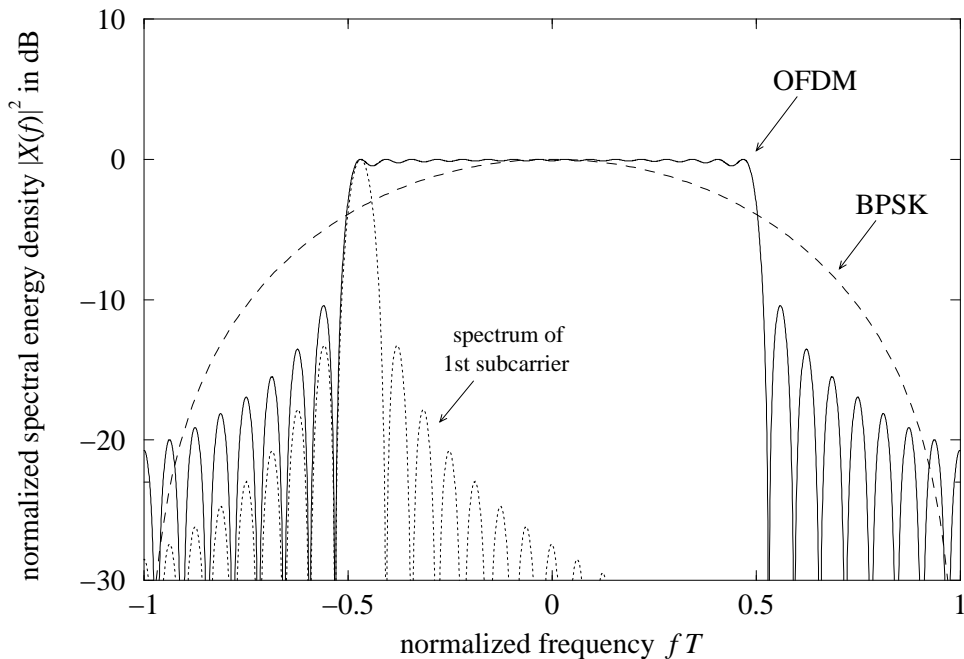


Figure 3.1: Normalized energy density spectrum versus normalized frequency  $fT$  of an OFDM symbol with  $N_c = 16$  subcarriers, of the first subcarrier, and of BPSK

diagram of an MC modulator employing OFDM based on an IDFT and MC demodulator employing inverse OFDM based on a DFT is illustrated in Fig. 3.2.

When the number of subcarriers increases, the OFDM symbol duration  $T_s$  becomes large compared to the duration of the impulse response  $\tau_{\max}$  of the channel and the amount of ISI reduces. However, to completely avoid the effect of ISI and, thus, to maintain the orthogonality between the signals on the  $N_c$  subcarriers, i.e., also to avoid ICI, a guard interval of duration

$$T_g \geq \tau_{\max} \quad (3.7)$$

has to be inserted between adjacent OFDM symbols [All87, Bin90, Pro95]. The guard interval is a cyclic prefix added to each OFDM symbol which is obtained by extending the duration of an OFDM symbol to

$$T'_s = T_g + T_s. \quad (3.8)$$

The discrete length of the guard interval has to be

$$L_g \geq \left\lceil \frac{\tau_{\max} N_c}{T_s} \right\rceil \quad (3.9)$$

samples to prevent ISI. The sampled sequence  $\{x_\nu\}$  with cyclic extended guard interval results in

$$x_\nu = \frac{1}{\sqrt{N_c}} \sum_{n=1}^{N_c} S_n e^{j2\pi(n-1)(\nu-1)/N_c}, \quad \nu = 1 - L_g, \dots, N_c. \quad (3.10)$$

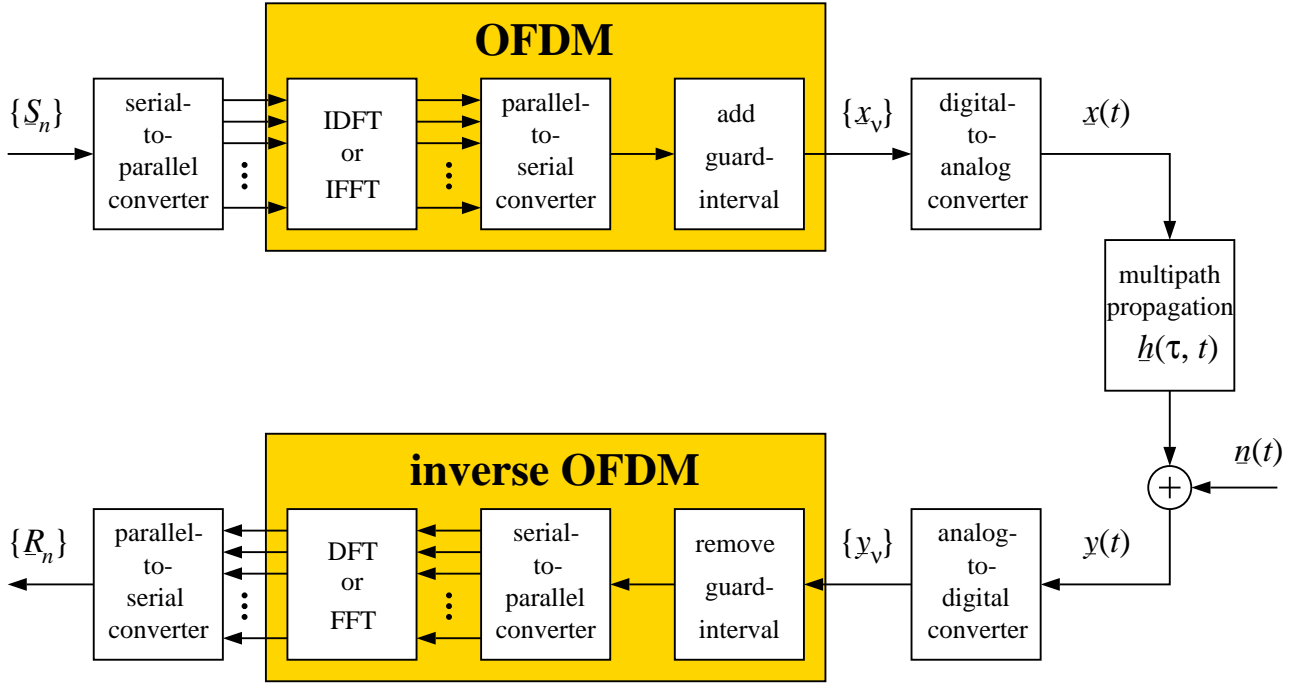


Figure 3.2: MC transmission system with OFDM

In practice, the sampled sequence  $\{\underline{x}_\nu\}$ ,  $\nu = 1 - L_g, \dots, N_c$ , is passed through a digital-to-analog converter whose output ideally would be the signal waveform  $\underline{x}(t)$  given in (3.3) with increased duration  $T'_s$ .

The output of the channel is the signal waveform  $\underline{y}(t)$  obtained from convolution of  $\underline{x}(t)$  with the channel impulse response  $\underline{h}(\tau, t)$  and addition of a noise signal  $\underline{n}(t)$ , i.e.,

$$\underline{y}(t) = \int_0^{\tau_{\max}} \underline{x}(t - \tau) \underline{h}(\tau, t) d\tau + \underline{n}(t). \quad (3.11)$$

The noise signal  $\underline{n}(t)$  contains the inherent disturbances of the transmission system, which are, motivated by the central limit theorem, modelled as additive white Gaussian noise (AWGN). The received signal  $\underline{y}(t)$  is passed through an analog-to-digital converter, whose output sequence  $\{\underline{y}_\nu\}$ ,  $\nu = 1 - L_g, \dots, N_c$ , is the received signal  $\underline{y}(t)$  sampled at rate  $N_c/T_s$ . Since ISI is only present in the first  $L_g$  samples of the received sequence, these  $L_g$  samples are removed before MC demodulation. The ISI-free part  $\nu = 1, \dots, N_c$  of  $\{\underline{y}_\nu\}$  is MC demodulated by inverse OFDM exploiting a DFT. The output of the DFT is the MC demodulated sequence  $\{\underline{R}_n\}$ ,  $n = 1, \dots, N_c$ , consisting of  $N_c$  complex-valued symbols

$$\underline{R}_n = \frac{1}{\sqrt{N_c}} \sum_{\nu=1}^{N_c} \underline{y}_\nu e^{-j2\pi(n-1)(\nu-1)/N_c}, \quad n = 1, \dots, N_c. \quad (3.12)$$

Since ICI can be avoided due to the guard interval, each subchannel can be considered separately. When, furthermore, assuming that the fading on each subchannel is flat and ISI is

removed, a received symbol  $\underline{R}_n$  is obtained from the frequency domain representation according to

$$\underline{R}_n = \underline{H}_n \underline{S}_n + \underline{N}_n, \quad n = 1, \dots, N_c, \quad (3.13)$$

where  $\underline{H}_n$  is the flat fading factor of the  $n$ th subcarrier and  $\underline{N}_n$  represents the AWGN of the  $n$ th subcarrier. The flat fading factor  $\underline{H}_n$  is the sample of the channel transfer function  $\underline{H}_{n,i}$  according to (2.26) at the  $n$ th subcarrier. The time index  $i$  is omitted for simplicity, as mentioned at the beginning of this section. The real and the imaginary parts of the noise components  $\underline{N}_n$ ,  $n = 1, \dots, N_c$ , are assumed to be statistically independent, Gaussian distributed random variables with zero-mean and equal variance. The variance of the noise is given by

$$\sigma^2 = E\{|\underline{N}_n|^2\}, \quad n = 1, \dots, N_c. \quad (3.14)$$

With the assumptions made in (3.13), the MC transmission system shown in Fig. 3.2 can be viewed as a discrete-time and -frequency transmission system with a set of  $N_c$  parallel Gaussian channels with different complex-valued attenuations according to Fig. 3.3.

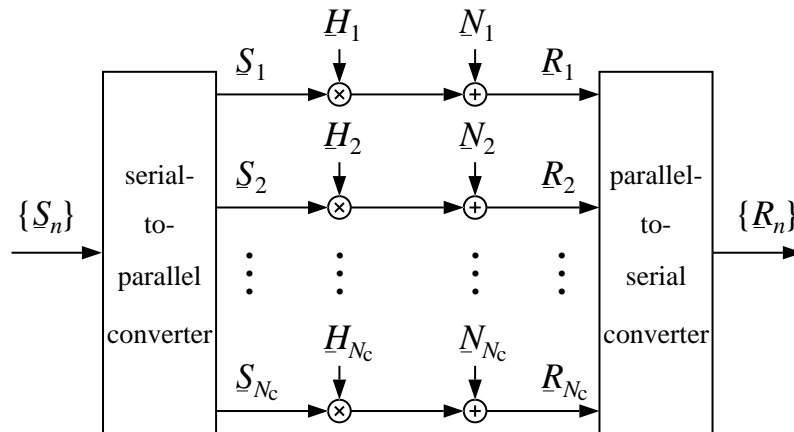


Figure 3.3: Simplified MC transmission system based on OFDM

The time/frequency representation of an OFDM symbol used in this thesis is shown in Fig. 3.4 a). A block of subsequent OFDM symbols, where the information transmitted within this OFDM symbols belongs together, e.g., due to coding and/or spreading in time and frequency direction, is referred to as an OFDM frame. An OFDM frame consisting of  $N_s$  OFDM symbols with frame duration

$$T_{\text{fr}} = N_s T'_s \quad (3.15)$$

is illustrated in Fig. 3.4 b). The time/frequency representation in Fig. 3.4 is obtained from the three-dimensional time/frequency/power density representation introduced in Section 1.2 by omitting the dimension of the power density.

In order to concisely describe OFDM and later on MC-CDMA, a matrix-vector notation is introduced. Vectors are represented by boldface small letters and matrices by boldface capital

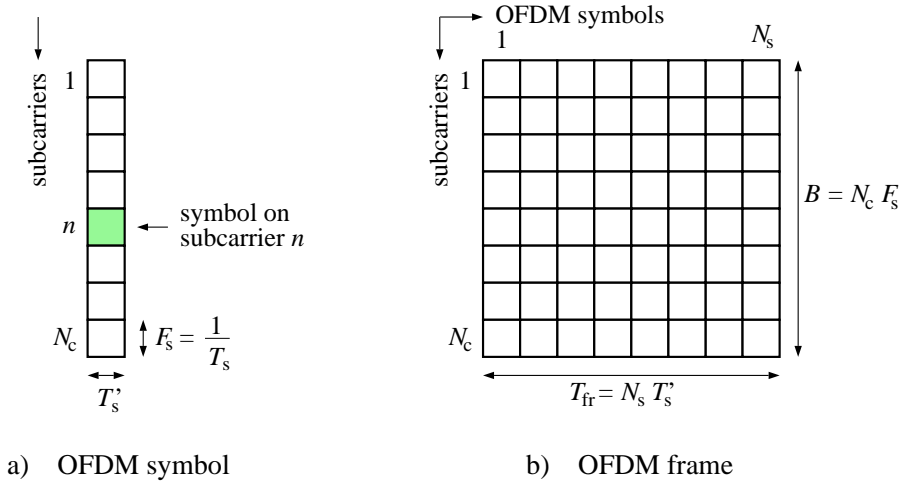


Figure 3.4: Time/frequency representation of an OFDM symbol and an OFDM frame

letters. The symbol  $(\cdot)^T$  denotes the transposition of a vector or a matrix. The sequence  $\{\underline{S}_n\}$ ,  $n = 1, \dots, N_c$ , of  $N_c$  source symbols transmitted in one OFDM symbol is represented by the vector

$$\underline{\mathbf{s}} = (\underline{S}_1, \underline{S}_2, \dots, \underline{S}_{N_c})^T \quad (3.16)$$

and the assigned received sequence  $\{\underline{R}_n\}$ ,  $n = 1, \dots, N_c$ , obtained after inverse OFDM is given by the vector

$$\underline{\mathbf{r}} = (\underline{R}_1, \underline{R}_2, \dots, \underline{R}_{N_c})^T. \quad (3.17)$$

With these notations, the received vector  $\underline{\mathbf{r}}$  is obtained from

$$\underline{\mathbf{r}} = \underline{\mathbf{H}} \underline{\mathbf{s}} + \underline{\mathbf{n}}, \quad (3.18)$$

where the  $N_c \times N_c$  channel matrix

$$\underline{\mathbf{H}} = \begin{pmatrix} \underline{H}_1 & 0 & \cdots & 0 \\ 0 & \underline{H}_2 & & 0 \\ \vdots & & \ddots & \vdots \\ 0 & 0 & \cdots & \underline{H}_{N_c} \end{pmatrix} \quad (3.19)$$

is of diagonal type due to the absence of ICI. The diagonal components of  $\underline{\mathbf{H}}$  are the complex-valued flat fading coefficients  $\underline{H}_n$ ,  $n = 1, \dots, N_c$ . The vector

$$\underline{\mathbf{n}} = (\underline{N}_1, \underline{N}_2, \dots, \underline{N}_{N_c})^T \quad (3.20)$$

represents the AWGN on the  $N_c$  subcarriers. Furthermore, the sequence  $\{\underline{x}_\nu\}$ ,  $\nu = 1 - L_g, \dots, N_c$ , of an OFDM symbol including the guard interval at the output of the MC modulator is given by the vector

$$\underline{\mathbf{x}} = (\underline{x}_{1-L_g}, \underline{x}_{2-L_g}, \dots, \underline{x}_{N_c})^T \quad (3.21)$$

and is the IDFT of the vector  $\underline{\mathbf{s}}$ , cf. (3.10). The received sequence  $\{y_\nu\}$ ,  $\nu = 1 - L_g, \dots, N_c$ , at the input of the MC demodulator including the guard interval is represented by the vector

$$\underline{\mathbf{y}} = (y_{1-L_g}, y_{2-L_g}, \dots, y_{N_c})^T. \quad (3.22)$$

The vector  $\underline{\mathbf{r}}$  given by (3.18) is the DFT of the vector  $\underline{\mathbf{y}}$  without guard interval, cf. (3.12).

The motivation for the use of OFDM in mobile radio applications is the possibility of realizing bandwidth-efficient systems with simple receivers. The necessary equalization in multipath channels can simply be realized by one complex-valued multiplication per subcarrier, treated in detail in Section 3.3. However, the following effects which may more or less degrade the system performance have to be taken into account when applying OFDM:

- The energy of a transmitted OFDM symbol increases due to the cyclically extended guard interval. The loss in energy in dB due to the guard interval is

$$V_{\text{guard}} = 10 \log_{10} \left( \frac{T_g}{T_s} + 1 \right). \quad (3.23)$$

Even if the guard interval is in the order of 20% of the total OFDM symbol duration  $T'_s$ , the loss  $V_{\text{guard}}$  is less than 1 dB. In this case, the loss in data rate due to the guard interval is 20%. However, single carrier systems have a similar loss in data rate due to pulse shaping with filter roll-offs of finite steepness. Thus, with respect to the ICI- and ISI-free data detection, the guard interval seems to be a good investment [ViF95, OrM97].

- An accurate frequency and time synchronization is required in MC systems [CIM94, PoM95, Rob97]. The investigation of synchronization errors in MC-CDMA mobile radio systems is not part of this work and the reader is referred to [ToK96a, ToK96b]. Time and frequency synchronization are assumed to be perfect within this thesis.
- The effect of phase noise caused by the imperfections of the transmitter and receiver oscillators substantially influence the system performance [RoK95, SSR95]. The influence of phase noise on the performance of MC-CDMA mobile radio systems is investigated in [ToK96a, StM97] and is not in the scope of this thesis.
- An OFDM symbol  $\underline{x}(t)$  is the sum of many independently modulated sinewaves and its envelope has an almost Gaussian distribution. This yields high peak-to-average power ratios and high demands on linear amplifiers. Nonlinearities in the amplifiers may cause ICI and if the amplifiers are not adapted with proper output backoff, the clipping distortion may cause severe performance degradations [SSR95, BCF96]. Possible counter-measures are predistortion of the transmitted signal with a complementary nonlinearity [Bin90] or, when considering MC-CDMA systems, an approach is to design spreading codes resulting in reduced dynamic ranges [AuF96]. Within this thesis, the amplifiers in the MC-CDMA mobile radio system are assumed to be linear and adapted with appropriate output backoff.

### 3.1.2 Principle of MC-FDMA, MC-TDMA, and MC-CDMA

The advantages of combining the multiple access schemes FDMA, TDMA, and DS-CDMA with MC modulation were discussed in Section 1.2.2. The principle of the arising MC-FDMA, MC-TDMA, and MC-CDMA schemes is depicted in Fig. 3.5 a), b), and c), respectively, for the case of two active users. In the case of MC-FDMA, one or several subcarriers are exclusively

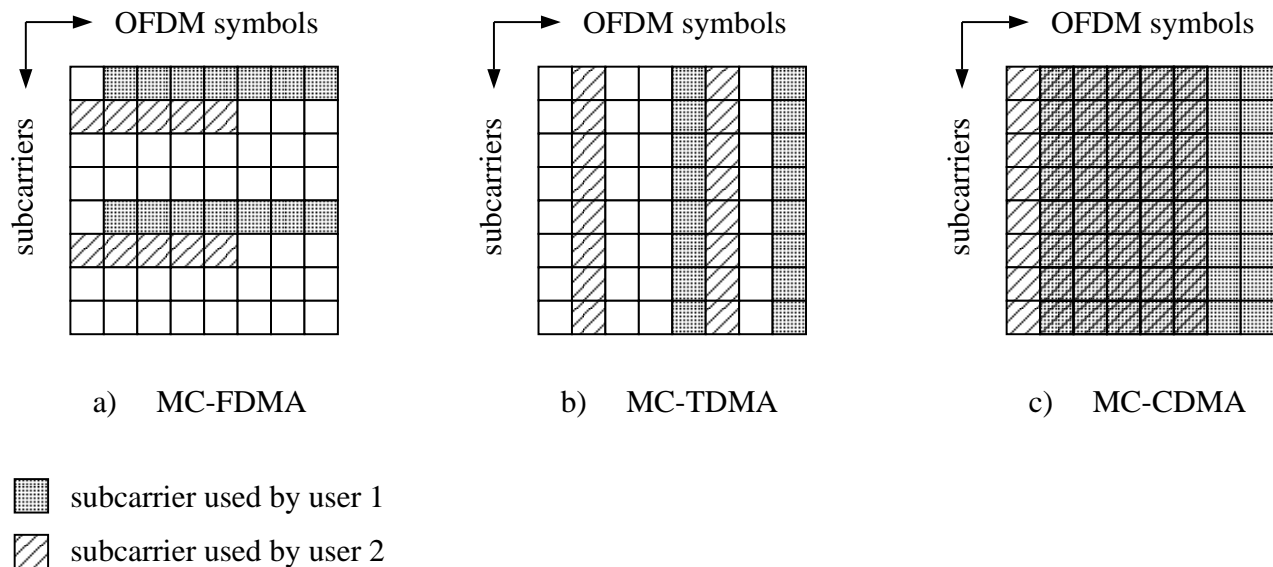


Figure 3.5: Multiple access schemes based on MC modulation; two active users

allocated to a user for transmission. In the case of MC-TDMA, the whole transmission bandwidth is exclusively allocated to a single user for a certain number of OFDM symbols. Thus, MC-FDMA and MC-TDMA can completely avoid MAI, ISI, and ICI. Assuming that adjacent source symbols are affected by fading independently to each other due to perfect interleaving, the performance of MC-FDMA and MC-TDMA systems or any hybrid combination of both is similar [Kai96]. With MC-CDMA different users share the same frequency band, i.e., the same subcarriers, at the same time. Hence, an MC-CDMA system has to cope with MAI and, thus, may perform quite differently from MC-FDMA and MC-TDMA systems. The performance of an uncoded and coded MC-FDMA and MC-TDMA system, respectively, with perfect interleaving is chosen as reference for the evaluation of the presented MC-CDMA system. In the next section the signal structure of MC-CDMA is introduced in detail.

## 3.2 MC-CDMA Signal Structure

The fundamentals of data symbol spreading with MC-CDMA introduced in Section 1.2.2 are pointed out in the three-dimensional time/frequency/power density representation of Fig. 1.4. The essential difference of data symbol spreading with MC-CDMA and data symbol spreading

with DS-CDMA is visualized in the comparison of Figs. 1.2 and 1.4. DS-CDMA signals are characterized by their multiple repetition of each data symbol due to the multiplication with the high rate spreading code in the time domain, where, in contrast, MC-CDMA signals are characterized by their multiple repetition of each data symbol due to the multiplication with a high rate spreading code in the frequency domain. Moreover, a DS-CDMA signal is typically designed to transmit the data modulated chips of a spreading code on adjacent time slots, whereas, an MC-CDMA signal transmits the data modulated chips of a spreading code on not necessarily neighbouring subcarriers, increasing the flexibility of the system. In this section, the MC-CDMA signal structure is described and the flexibility due to the spreading code structure in the frequency domain is pointed out. The number of simultaneously active users in the MC-CDMA mobile radio system is  $K$ . Values and functions related to the  $k$ th user, where  $k$  may take on the values  $1, \dots, K$ , are marked by an index  $(k)$ . All statements for values and functions with the index  $(k)$  are valid for each  $k, k = 1, \dots, K$ .

The generation of an MC spread spectrum signal is illustrated in Fig. 3.6 and is applicable on the transmitter side in both the up- and the down-link. The serial concatenation of DS

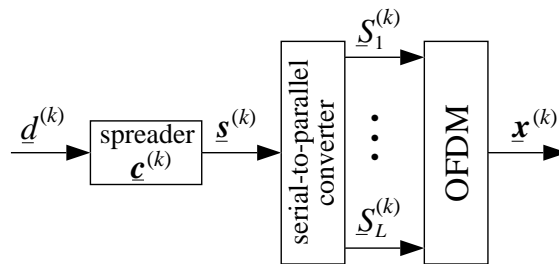


Figure 3.6: MC spread spectrum signal generation

spreading, cf. Fig. 1.2, and MC modulation, cf. Fig. 1.3, is shown, however, the equivalent realization illustrated in Fig. 1.4 is also applicable. The transmission of a complex-valued data symbol  $\underline{d}^{(k)}$  of the  $k$ th user is shown in Fig. 3.6. The data symbol  $\underline{d}^{(k)}$  to be transmitted over the radio channel is taken from the complex data symbol alphabet

$$V_d = \{v_{d,1}, v_{d,2}, \dots, v_{d,M_d}\} \quad (3.24)$$

of size  $M_d$ . The data symbol  $\underline{d}^{(k)}$  is obtained after symbol mapping, where  $\log_2(M_d)$  data bits are mapped into a complex-valued data symbol  $\underline{d}^{(k)}$  [Pro95]. The data symbol rate is  $1/T_d$ . For brevity, but without loss of generality, the MC-CDMA signal generation is described for a single data symbol per user as far as possible, by omitting an otherwise necessary data symbol index. In the transmitter, the data symbol  $\underline{d}^{(k)}$  is multiplied and, thus, marked with the user specific spreading code

$$\underline{\mathbf{c}}^{(k)} = (C_1^{(k)}, C_2^{(k)}, \dots, C_L^{(k)})^T \quad (3.25)$$

of the  $k$ th user. The chips  $C_l^{(k)}$ ,  $l = 1, \dots, L$ , are taken from the complex chip alphabet

$$V_c = \{v_{c,1}, v_{c,2}, \dots, v_{c,M_s}\} \quad (3.26)$$

of size  $M_s$ , where  $M_s$  is not necessarily equal to  $M_d$ . The chip rate of the serial spreading code  $\mathbf{c}^{(k)}$  before serial-to-parallel conversion is

$$\frac{1}{T_c} = \frac{L}{T_d} \quad (3.27)$$

and is  $L$  times higher than the data symbol rate  $1/T_d$ . The complex-valued sequence obtained from the multiplication of a data symbol  $\underline{d}^{(k)} \in \mathcal{V}_d$ , cf. (3.24), with the assigned spreading code  $\mathbf{c}^{(k)}$  is given by the vector

$$\mathbf{s}^{(k)} = \underline{d}^{(k)} \mathbf{c}^{(k)} = (\underline{S}_1^{(k)}, \underline{S}_2^{(k)}, \dots, \underline{S}_L^{(k)})^T. \quad (3.28)$$

The rate of the components  $\underline{S}_l^{(k)}$ ,  $l = 1, \dots, L$ , before serial-to-parallel conversion is  $1/T_c$ . It should be noted that the transmission of  $\mathbf{s}^{(k)}$  with single-carrier modulation conforms with the principle of DS spread spectrum according to Fig. 1.2. An MC-CDMA signal is obtained after modulating the components  $\underline{S}_l^{(k)}$ ,  $l = 1, \dots, L$ , in parallel onto  $L$  subcarriers according to (3.10) [FaP93, YLF93, CBJ93]. Thus, each data symbol  $\underline{d}^{(k)}$  is spread over  $L$  subcarriers. The duration of an MC modulated component  $\underline{S}_l^{(k)}$ ,  $l = 1, \dots, L$ , is equal to the OFDM symbol duration, which, including the guard interval, is

$$T'_s = T_g + N_c T_c. \quad (3.29)$$

The transmission of one data symbol per user per OFDM symbol requires

$$N_c = L \quad (3.30)$$

subcarriers. In this case, the OFDM symbol duration including the guard interval is

$$T'_s = T_g + T_d. \quad (3.31)$$

An MC-CDMA system designed for the transmission of one data symbol per user per OFDM symbol is referred to as a basic MC-CDMA system in the following. When applying orthogonal spreading codes  $\mathbf{c}^{(k)}$  like Walsh-Hadamard codes, the maximum number of active users  $K_{\max}$  in the basic MC-CDMA system corresponds to the spreading code length  $L$ , i.e.,

$$K_{\max} = L. \quad (3.32)$$

With fully loaded basic MC-CDMA system according to (3.32) and taking into account that  $K_{\max}$  is upper bounded by the receiver complexity, the number of subcarriers  $N_c$  is also upper bounded by  $K_{\max}$ , cf. (3.32) and (3.30). To support large numbers of users while having a low receiver complexity and, furthermore, to use MC-CDMA systems with a sufficiently large number of subcarriers to guarantee flat fading per subchannel, modifications of the basic MC-CDMA system are necessary [FaP93, Faz93]. In the following, appropriate modifications of the basic MC-CDMA system are introduced and explained for the downlink of a mobile radio system. The downlink is chosen, since this scenario enables a better illustration of the modifications than the uplink. It has to be mentioned that this modifications are also suitable in the uplink of an MC-CDMA mobile radio system.

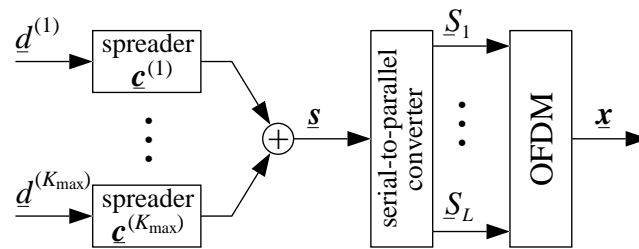


Figure 3.7: Basic MC-CDMA transmitter for the downlink; BS with  $K_{\max} = L$  active users and  $N_c = L$  subcarriers

Generally, when considering the downlink of an MC-CDMA system, it is computationally efficient to add the signals of the  $K$  users in the transmitter before serial-to-parallel conversion, as depicted in Fig. 3.7 for a basic MC-CDMA transmitter. Thus, OFDM has to be carried out only once per OFDM symbol for all users. The case with the maximum number of active users, i.e., with a fully loaded system, is shown with the intention to straightforwardly derive the MC-CDMA system modifications. The data symbol and, thus, chip synchronous superposition of the  $K_{\max}$  vectors  $\underline{s}^{(k)}$ ,  $k = 1, \dots, K_{\max}$ , yields the vector

$$\underline{s} = \sum_{k=1}^{K_{\max}} \underline{s}^{(k)} = (S_1, S_2, \dots, S_L)^T. \quad (3.33)$$

The three MC-CDMA system modifications presented in the following are in this thesis referred to as  $M$ -Modification,  $Q$ -Modification, and  $M\&Q$ -Modification. The  $M$ -Modification and the  $Q$ -Modification are introduced as basic components of the  $M\&Q$ -Modification. An MC-CDMA system with  $M\&Q$ -Modification correspond to the MC-CDMA system concept considered in [FaP93, Faz93]. Since the  $M$ -Modification and the  $Q$ -Modification are independent from each other, they can be applied individually also.

**$M$ -Modification:** The intention of the  $M$ -Modification is to increase the number of subcarriers while maintaining constant the spreading code length and the maximum number of active users. Consequently, the OFDM symbol duration increases and the loss in bandwidth efficiency due to the guard interval decreases. Moreover, the tighter subcarrier spacing enables one to guarantee flat fading per subchannel in propagation scenarios with decreased coherence bandwidth. With the  $M$ -Modification, each user transmits simultaneously  $M$  greater than 1 data symbols per OFDM symbol. The total number of subcarriers of the modified MC-CDMA system is

$$N_c = ML. \quad (3.34)$$

Each user exploits the total of  $N_c$  subcarriers for data transmission. The OFDM symbol duration including the guard interval increases to

$$T'_s = T_g + MLT_c, \quad (3.35)$$

where it can be observed that the loss in bandwidth efficiency due to the guard interval decreases with increasing  $M$ . The maximum number of active users is still defined according to

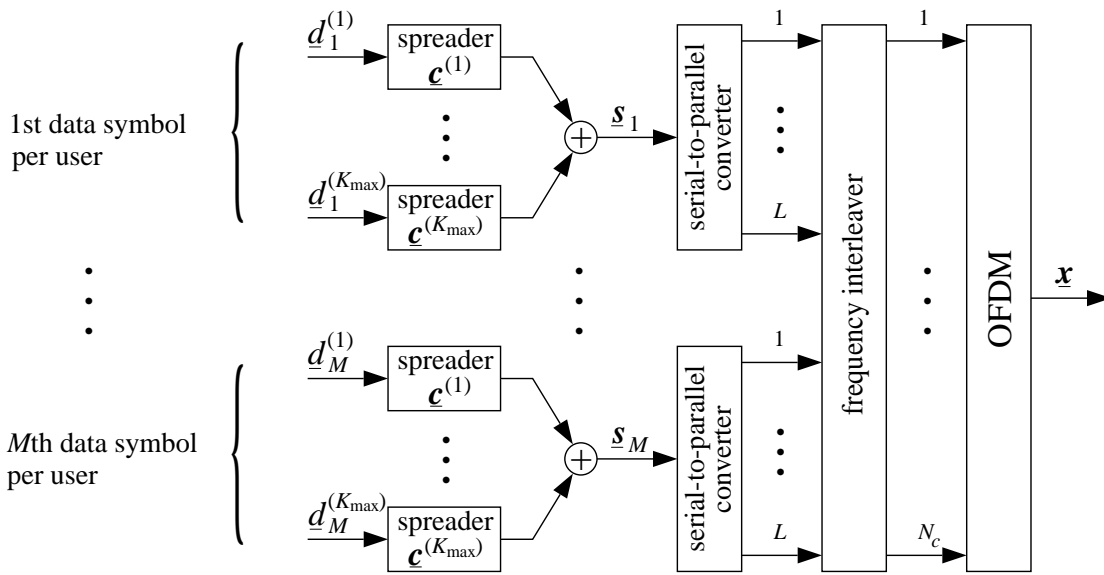


Figure 3.8: *M*-Modification: MC-CDMA transmitter with simultaneous transmission of *M* data symbols per user and OFDM symbol; BS with  $K_{\max} = L$  active users and  $N_c = ML$  subcarriers

(3.32). The assigned MC-CDMA transmitter is shown in Fig. 3.8. The data symbol index  $m$ ,  $m = 1, \dots, M$ , is introduced in Fig. 3.8 to distinguish the  $M$  simultaneously transmitted data symbols  $d_m^{(k)}$ ,  $m = 1, \dots, M$ , of the  $k$ th user. The number  $M$  is upper limited by the coherence time  $(\Delta t)_c$  of the channel, cf. (2.13), since the symbol duration  $T'_s$ , which increases with increasing  $M$ , has to be smaller than  $(\Delta t)_c$  to guarantee that the channel is time-invariant during one OFDM symbol duration.

To optimally exploit frequency diversity, the components of the sequences  $\mathbf{s}_m$ ,  $m = 1, \dots, M$ , transmitted in the same OFDM symbol are interleaved over the frequency. Subcarriers used for the transmission of  $\mathbf{s}_m$  should have a spacing greater than the coherence bandwidth of the channel. Thus, the components of one sequence  $\mathbf{s}_m$  are affected independently, reducing the probability that  $\mathbf{s}_m$  is completely located in a deep fade. The interleaving is carried out prior to OFDM. The frequency interleaver can be a block interleaver which guarantees the maximum frequency separation between the components of  $\mathbf{s}_m$ . However, due to a possible periodicity of the fading process in frequency, the block interleaver can fail if the periodicity is similar to the frequency separation between adjacent components. This effect can be reduced if a pseudo-random frequency interleaver is used.

**Q-Modification:** The intention of the *Q*-Modification is to reduce the receiver complexity by reducing the spreading code length per user, while maintaining constant the maximum number of active users and the number of subcarriers. The complexity of an MC-CDMA receiver with SD increases with increasing spreading code length  $L$ . In the case of MD, the complexity of an MC-CDMA receiver increases with both increasing spreading code length  $L$  and increasing number of active users  $K$ . If, for instance, JD with MLSE should be applied in the receiver,

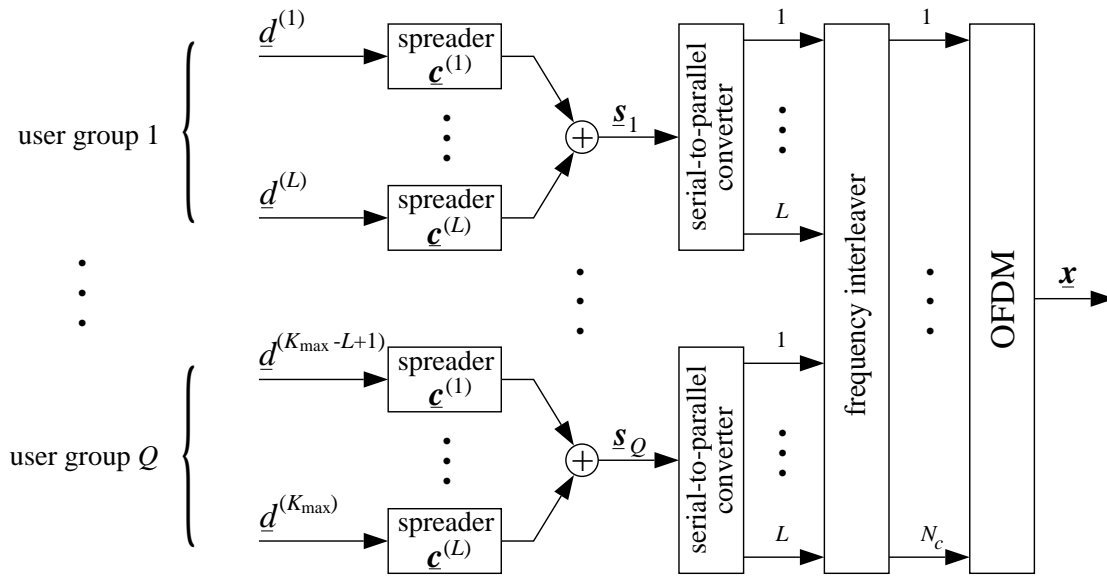


Figure 3.9:  $Q$ -Modification: MC-CDMA transmitter with  $Q$  independent user groups; BS with  $K_{\max} = QL$  active users and  $N_c = QL$  subcarriers

the number of simultaneously active users is limited to  $K$  less than 10 due to computational complexity [Pro95]. To keep the complexity of the receiver to an acceptable level by nevertheless allowing large numbers of active users, the basic MC-CDMA transmitter has to be modified as depicted in Fig. 3.9. The users are subdivided in  $Q$  independent user groups, where each user group  $q$ ,  $q = 1, \dots, Q$ , exploits its own  $L$  subcarriers within its subsystem. The  $Q$ -Modification introduces an additional FDMA component on subcarrier level in the transmission scheme, resulting in a hybrid MC-CDMA mobile radio system. A single subsystem is comparable to the basic MC-CDMA transmitter illustrated in Fig. 3.7. The number of active users in the  $q$ th subsystem is  $K_q$  and the maximum number of active users in the  $q$ th subsystem is

$$K_{q,\max} = L \quad (3.36)$$

The total number of simultaneously active users in the MC-CDMA system is

$$K = \sum_{q=1}^Q K_q, \quad (3.37)$$

and the maximum number of active users results in

$$K_{\max} = \sum_{q=1}^Q K_{q,\max} = QL. \quad (3.38)$$

While maintaining the maximum number of supplied users constant, the required spreading code length decreases proportional to  $Q$ . This enables a significant reduction of the receiver complexity, since in the receiver, only the data symbols of the assigned subsystem have to be detected. The number of subcarriers of the modified scheme is

$$N_c = QL, \quad (3.39)$$

where each user only exploits a subset of  $L$  subcarriers for data transmission due to the FDMA component introduced by the  $Q$ -Modification. To nevertheless optimally exploit the frequency diversity of the channel, the components of the spread sequences  $\mathbf{s}_q$ ,  $q = 1, \dots, Q$ , are interleaved over the frequency, comparable to the frequency interleaving applied with the  $M$ -Modification. The OFDM symbol duration including the guard interval is

$$T'_s = T_g + QLT_c. \quad (3.40)$$

It has to be mentioned that only one set of  $L$  orthogonal spreading codes of length  $L$  is required within the whole MC-CDMA system. This set of spreading codes is used in each subsystem, cf. Fig. 3.9.

**$M\&Q$ -Modification:** The  $M\&Q$ -Modification is a combination of the  $M$ - and the  $Q$ -Modification, resulting in an MC-CDMA system with adjustable number of subcarriers and receiver complexity, keeping constant the maximum number of active users. The transmission of  $M$  data symbols per user and, additionally, the splitting of the users in  $Q$  independent user groups according to the  $M\&Q$ -Modification is illustrated in Fig. 3.10. The total number of subcarriers used by the MC-CDMA system with  $M\&Q$ -Modification is

$$N_c = QML, \quad (3.41)$$

where each user only exploits a subset of  $ML$  subcarriers for data transmission due to the FDMA component introduced by the  $Q$ -Modification. The maximum number of active users is given by (3.38). The total OFDM symbol duration including the guard interval results with the  $M\&Q$ -Modification in

$$T'_s = T_g + QMLT_c. \quad (3.42)$$

A frequency interleaver scrambles the information of all subsystems prior OFDM to guarantee an optimum exploitation of the frequency diversity offered by the mobile radio channel.

As mentioned before, the  $Q$ -, the  $M$ -, and the  $M\&Q$ -Modifications are also suitable for the uplink of an MC-CDMA mobile radio system. For the  $Q$ - and  $M\&Q$ -Modification in the uplink only the inputs of the frequency interleaver of the user group of interest are connected in the transmitter, all other inputs are set to zero.

Finally, it has to be noted that an MC-CDMA system with its basic implementation or with any of the three modifications presented in this section supports an additional TDMA component in the up- and in the downlink, since the transmission is synchronized on OFDM symbols [KaH97a]. The additional flexibility due to a TDMA component in an MC-CDMA system is exploited in the system design presented in Chapter 6.

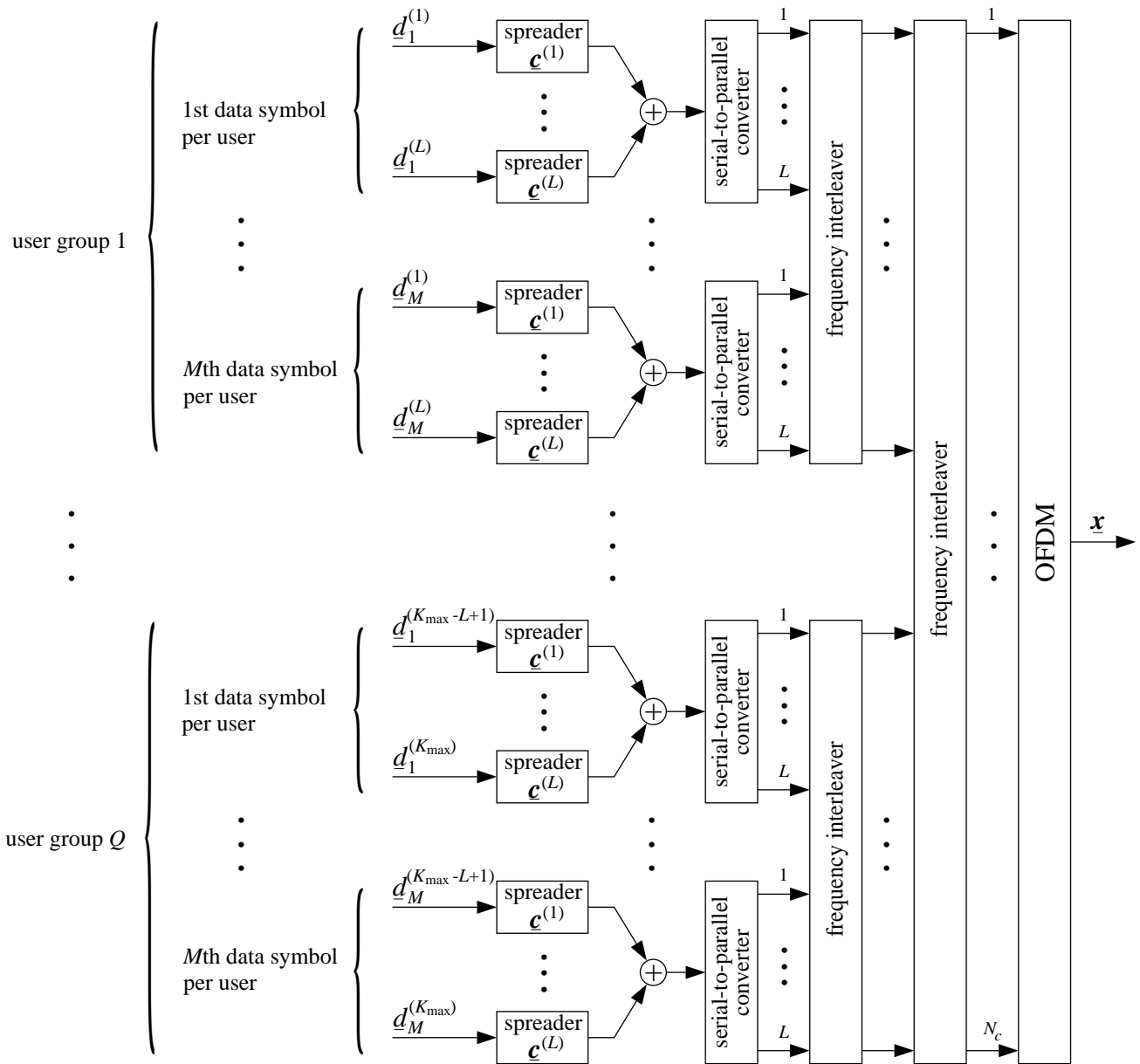


Figure 3.10:  $M$  &  $Q$ -Modification: MC-CDMA transmitter with  $Q$  independent user groups and simultaneous transmission of  $M$  data symbols per user and OFDM symbol; BS with  $K_{\max} = QL$  active users and  $N_c = QML$  subcarriers

### 3.3 MC-CDMA Data Detection Techniques

#### 3.3.1 Introduction

The MC-CDMA signal structure introduced in the previous section enables the realization of powerful receivers with low complexity due to the avoidance of ISI and ICI in the detection process. This advantage can be exploited in the up- and in the downlink of a mobile radio system. However, especially in the downlink, the requirements with respect to weight, size, and cost and, therefore, to low complexity while still guaranteeing high bandwidth and power efficiency are more severe for the mobile receiver than for the BS. In the BS more complex receivers are tolerable. This thesis mainly focuses on the high demands on the mobile receiver in the downlink and presents in this section data detection techniques especially designed for the downlink. An appropriate uplink concept employing MC modulation in combination with the spread spectrum technique is presented and investigated in Appendix B.

The data detection considered in the sequel includes all components such as equalizer, quantizer, etc., which are necessary to get a hard or a soft decided value about the transmitted data symbol. The investigated combining techniques MRC and EGC, which combine the received signal components but not try to equalize the received signal, are also part of the data detection. The data detection techniques analyzed in this section are suitable for MC-CDMA mobile radio systems with any of the modifications presented in the previous section. Since the data detection between the different subsystems is independent from each other and since due to frequency interleaving the performance in all subsystems is similar, it is sufficient to focus on the data detection in one arbitrary subsystem. The mobile MC-CDMA receiver with SD or MD, respectively, for the data of the  $k$ th user transmitted in one subsystem is depicted in Fig. 3.11.

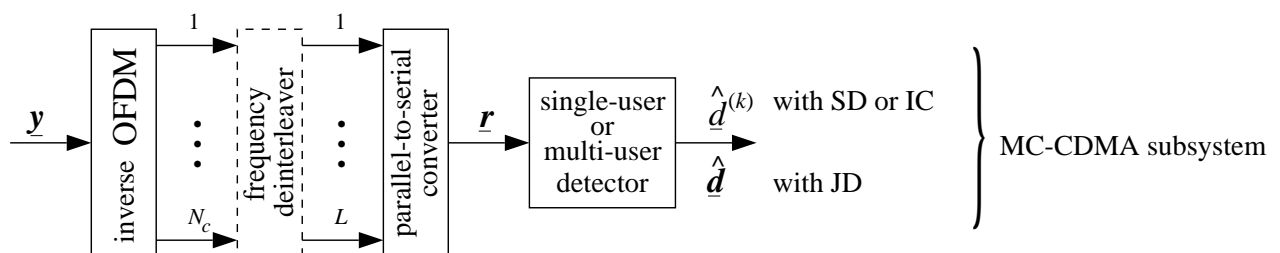


Figure 3.11: MC-CDMA receiver with data detection of the  $k$ th user in one subsystem

The relation between the number of subcarriers  $N_c$  and the spreading code length  $L$  depends on whether the basic MC-CDMA system, cf. (3.30), or a modified MC-CDMA system, cf. (3.34), (3.39), and (3.41), respectively, is considered.

In the following, the data symbol and user group indices  $m$ ,  $m = 1, \dots, M$ , and  $q$ ,  $q = 1, \dots, Q$ , respectively, are omitted for brevity. Only the notation of the number of users in a subsystem

$K_q$  and  $K_{q,\max}$ , respectively, is further used with the purpose of emphasizing that the total number of users  $K$  and  $K_{\max}$ , respectively, of the whole MC-CDMA system is in general much higher than  $K_q$  and  $K_{q,\max}$ , respectively. Moreover, equations defined with the variable  $K_q$  instead of  $K$  are valid for systems with and without  $Q$ -Modification.

The received sequence given by the vector  $\mathbf{y}$ , cf. (3.22), yields in the basic MC-CDMA receiver after inverse OFDM the vector  $\mathbf{r}$  defined according to (3.18). If either the  $M$ -, the  $Q$ -, or the  $M\&Q$ -Modification is used, an additional frequency deinterleaver is applied after inverse OFDM. At the output of the frequency deinterleaver the vector

$$\mathbf{r} = \mathbf{H}\mathbf{s} + \mathbf{n} = (\underline{R}_1, \underline{R}_2, \dots, \underline{R}_L)^T, \quad (3.43)$$

assigned to one MC-CDMA subsystem, is obtained. The transmitted vector  $\mathbf{s}$ , the received vector  $\mathbf{r}$ , the channel matrix  $\mathbf{H}$ , and the noise vector  $\mathbf{n}$  correspond to (3.16), (3.17), (3.19), and (3.20), respectively, except for the subcarrier index  $n$ ,  $n = 1, \dots, N_c$ , which is exchanged by the spreading code index  $l$ ,  $l = 1, \dots, L$ , since in a modified MC-CDMA system  $\mathbf{s}$  is transmitted only on a subset of the  $N_c$  subcarriers. The components of the channel matrix  $\mathbf{H}$  and of the noise vector  $\mathbf{n}$  in (3.43) represent the fading and noise, respectively, of the subcarriers where  $\mathbf{s}$  was transmitted on. Hence, if frequency interleaving is applied, it is taken into account in (3.43). The vector  $\mathbf{r}$  is processed in the data detector. The purpose of data detection is to get an estimate of the transmitted data symbol  $\underline{d}^{(k)}$  of the  $k$ th user. The estimate obtained after data detection can be a soft decided value or a hard decided value. This section evaluates SD and MD techniques in an uncoded MC-CDMA system and focuses on hard decided values. In Chapter 4, the optimum soft decided value of  $\underline{d}^{(k)}$  is derived for MC-CDMA systems with channel coding exploiting soft decision decoding.

With SD or MD applying IC, a hard decided value  $\hat{\underline{d}}^{(k)}$  for the transmitted data symbol  $\underline{d}^{(k)}$  of the  $k$ th user is obtained at the output of the data detector.

With MD applying JD, additionally the data symbol vector

$$\mathbf{d} = (\underline{d}^{(1)}, \underline{d}^{(2)}, \dots, \underline{d}^{(K_q)})^T \quad (3.44)$$

is introduced, representing the data symbols of the  $K_q$  users, simultaneously transmitted per OFDM symbol in one subsystem. Furthermore, the  $L \times K_q$  spreading code matrix containing the spreading codes of the  $K_q$  users is defined as

$$\mathbf{C} = (\underline{c}^{(1)} \ \underline{c}^{(2)} \ \dots \ \underline{c}^{(K_q)}) = \begin{pmatrix} \underline{C}_1^{(1)} & \underline{C}_1^{(2)} & \dots & \underline{C}_1^{(K_q)} \\ \underline{C}_2^{(1)} & \underline{C}_2^{(2)} & & \underline{C}_2^{(K_q)} \\ \vdots & & \ddots & \vdots \\ \underline{C}_L^{(1)} & \underline{C}_L^{(2)} & \dots & \underline{C}_L^{(K_q)} \end{pmatrix}, \quad (3.45)$$

where in the case of orthogonal spreading codes,  $K_q$  is equal to or less than  $L$ . The transmission vector  $\mathbf{s}$  defined in (3.33) can be rewritten as

$$\mathbf{s} = \mathbf{C}\mathbf{d} = (\underline{S}_1, \underline{S}_2, \dots, \underline{S}_L)^T. \quad (3.46)$$

The  $K_q$  hard decided values obtained with JD in one detection step are given by the vector

$$\hat{\mathbf{d}} = (\hat{d}^{(1)}, \hat{d}^{(2)}, \dots, \hat{d}^{(K_q)})^T. \quad (3.47)$$

The average SNR per subcarrier at the input of the receiver is defined as

$$\gamma_c = \frac{\mathbb{E}\{|H_l S_l|^2\}}{\sigma^2}, \quad (3.48)$$

where  $H_l$  represents the sample of the channel transfer function  $H_{n,i}$  according to (2.26) at the subcarrier where  $S_l$  was transmitted on. The time index  $i$  is omitted for brevity, as mentioned in Section 3.1.1. In the case of frequency interleaving, the index  $l$  and the index  $n$  are related by the interleaving function. In the basic MC-CDMA system without frequency interleaving,  $l$  is equal to  $n$ . Moreover,  $\sigma^2$  is the variance of the noise according to (3.14). When assuming that the channel is power normalized, i.e.,

$$\mathbb{E}\{|H_l|^2\} = 1, \quad (3.49)$$

and  $H_l$  is statistically independent of  $S_l$  for all  $l$ , the average SNR per subcarrier results in

$$\gamma_c = \frac{\mathbb{E}\{|S_l|^2\}}{\sigma^2} \Big|_{\mathbb{E}\{|H_l|^2\}=1}. \quad (3.50)$$

In this thesis, it is assumed that in the downlink the data symbols of all users have the same average energy or, correspondingly, have the same second moment  $\mathbb{E}\{|d^{(k)}|^2\}$  per user. Hence, the SNR per data symbol  $\gamma_s$  is related to the SNR per subcarrier  $\gamma_c$  by

$$\gamma_s = \frac{L \gamma_c}{K_q} = \frac{\mathbb{E}\{|d^{(k)}|^2\}}{\sigma^2} \Big|_{\mathbb{E}\{|H_l|^2\}=1}. \quad (3.51)$$

The average SNR per subcarrier  $\gamma_c$  is the  $L$ th fraction of  $\gamma_s$  due to the spreading of  $d^{(k)}$  over  $L$  subcarriers, multiplied with  $K_q$  since the signals of  $K_q$  users superpose. The average SNR per source bit  $\gamma_b$  is related to the average SNR per data symbol  $\gamma_s$  by

$$\gamma_b = \frac{\gamma_s}{R \log_2 M_d}, \quad (3.52)$$

where  $R$  is the channel code rate. The channel code rate  $R$  is defined as the ratio

$$R = \frac{L_a}{L_b}, \quad (3.53)$$

where  $L_a$  is the number of source bits and  $L_b$  is the number of resulting code bits at the output of the channel encoder. In the uncoded case  $R$  is equal to 1.

Information about the SNR at the input of the receiver is required for some detection techniques, for the computation of log-likelihood ratios when applying soft decision decoding, and for channel estimation. The SNR can be estimated with the pilot symbols transmitted for channel estimation and synchronization and by transmitting a null-symbol [FKR95], i.e., an OFDM symbol without signal energy, for instance at the beginning of each OFDM frame. In this thesis, the knowledge about the SNR in the receiver is assumed to be perfect.

### 3.3.2 Single-User Detection

The approach with SD detects the user signal of interest by not taking into account any information about the MAI. A scheme with SD of the data symbols of the  $k$ th user is shown in Fig. 3.12. After inverse OFDM and frequency deinterleaving, the received sequence  $\mathbf{r}$ , cf. (3.43),

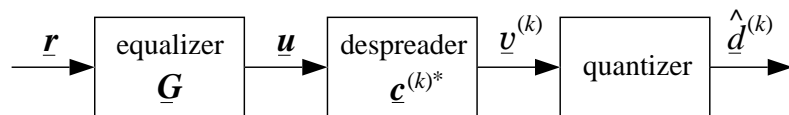


Figure 3.12: SD scheme

is equalized by employing a bank of adaptive one tap equalizers to combat the phase and amplitude distortions caused by the mobile radio channel on the subcarriers. The one tap equalizer is simply realized by one complex-valued multiplication per subcarrier. The term equalizer is generalized in the following, since the processing of the received vector  $\mathbf{r}$  according to typical diversity combining techniques is also investigated with the SD scheme shown in Fig. 3.12. The received sequence at the output of the equalizer has the form

$$\mathbf{u} = \mathbf{G} \mathbf{r} = (U_1, U_2, \dots, U_L)^T. \quad (3.54)$$

The diagonal equalizer matrix

$$\mathbf{G} = \begin{pmatrix} G_1 & 0 & \cdots & 0 \\ 0 & G_2 & & 0 \\ \vdots & & \ddots & \vdots \\ 0 & 0 & \cdots & G_L \end{pmatrix} \quad (3.55)$$

of dimension  $L \times L$  represents the  $L$  complex-valued equalizer coefficients of the subcarriers where  $\mathbf{s}$  was transmitted on. The complex-valued output  $\mathbf{u}$  of the equalizer is despread by correlating it with the conjugate complex user specific spreading code  $\mathbf{c}^{(k)*}$ , cf. (3.25). The complex-valued soft decided value at the output of the despreader is

$$\underline{v}^{(k)} = \mathbf{c}^{(k)*} \mathbf{u}^T. \quad (3.56)$$

The hard decided value  $\hat{d}^{(k)}$  of the detected data symbol is given by

$$\hat{d}^{(k)} = Q\{\underline{v}^{(k)}\}. \quad (3.57)$$

The quantization operation  $Q\{\cdot\}$  assigns to each soft decided value  $\underline{v}^{(k)}$  an element of the data symbol alphabet  $V_d$ , cf. (3.24).

With the assumptions made in (3.13), the uncoded MC-CDMA system with SD can be represented according to Fig. 3.13. In the case of the basic MC-CDMA implementation, the number

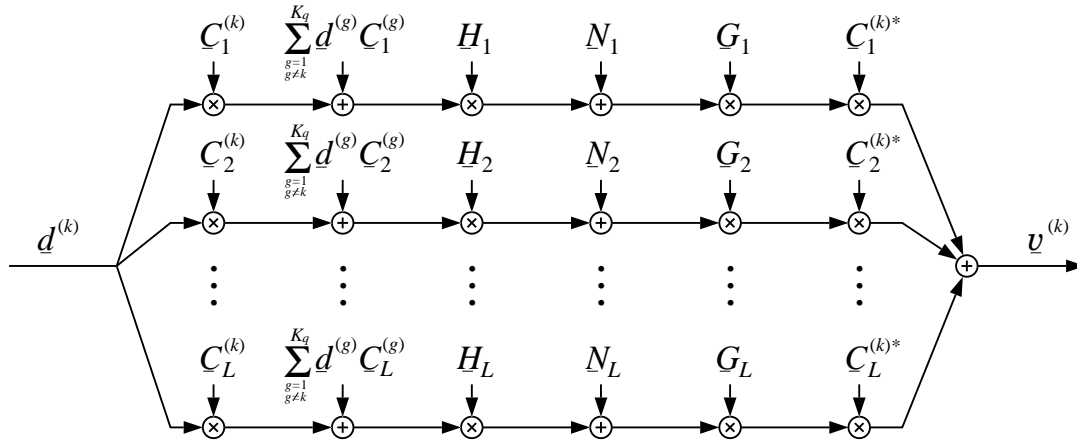


Figure 3.13: Simplified MC-CDMA system

of subcarriers  $N_c$  is equal to the spreading code length  $L$  in Fig. 3.13. If any of the modifications presented in Section 3.2 is used, only an MC-CDMA subsystem is shown in Fig. 3.13, and the total number of subcarriers  $N_c$  is greater than the spreading code length  $L$ . In the following, different strategies of selecting the equalizer coefficients  $G_l$ ,  $l = 1, \dots, L$ , are presented, where all statements for values and functions with the index  $l$  are valid for each  $l$ ,  $l = 1, \dots, L$ .

**Maximum Ratio Combining (MRC):** MRC is the optimum diversity combining technique with respect to the BER, if multiple replicas of the same information bearing signal, received over different diversity branches, are available at the receiver [Pro95, Stü96]. With MRC, the diversity branches are weighted by their respective conjugate complex channel coefficients, leading to

$$G_l = H_l^*. \quad (3.58)$$

The variance  $\sigma^2$  of the noise per branch is assumed to be the same, cf. (3.14). MRC is only conditionally applicable as an MC-CDMA detection technique. The  $L$  components of  $\mathbf{s}^{(k)}$  simultaneously transmitted on the  $L$  subcarriers contain the information of the same data symbol. However, each component of  $\mathbf{s}^{(k)}$  is weighted with the assigned chip of the spreading code before transmission, to achieve orthogonality between the sequences  $\mathbf{s}^{(k)}$ ,  $k = 1, \dots, K_q$ , which are simultaneously transmitted on the same subcarriers. This orthogonality is lost in the mobile radio channel by affecting the assigned subcarriers with different channel coefficients  $H_l$ ,  $l = 1, \dots, L$ . Therefore, by applying MRC according to (3.58), the orthogonality between the spreading codes  $\mathbf{c}^{(k)}$ ,  $k = 1, \dots, K_q$ , is further destroyed. Thus, MRC applied as MC-CDMA detection technique results in enhanced MAI. However, in the uplink where the user signals do not superimpose in an orthogonal fashion in a multipath channel, MRC is the most promising SD technique for MC-CDMA systems [YLF93].

In the single user case, MRC provides the best performance, since, due to the absence of MAI, the optimal diversity combining scenario is given. Thus, the BER with MRC for  $K_q$  equal to 1 is identical to the matched filter (MF) bound, which is the lower bound of the BER  $P_b$  of

any data detector [Pro95]. Based on this fact, it is shown in Section 3.3.3 that MRC may be of interest for the second and subsequent stages in a multistage detector based on IC, where after the first IC stage most of the MAI should be cancelled.

**Equal Gain Combining (EGC):** EGC is a diversity combining technique which, in contrast to MRC, weights all diversity branches, i.e. used subcarriers, with unit amplitude [Stü96]. With EGC, each branch is corrected in its phase by choosing

$$\underline{G}_l = \frac{\underline{H}_l^*}{|\underline{H}_l|}. \quad (3.59)$$

The MAI enhancement caused by (3.58) can be avoided with EGC.

**Zero-Forcing (ZF) Equalization:** ZF equalization, also known as orthogonality restoring combining (ORC) or channel inversion, can completely eliminate the MAI by restoring the orthogonality between the user specific spreading codes with an equalization coefficient chosen as

$$\underline{G}_l = \frac{1}{\underline{H}_l}, \quad (3.60)$$

corresponding to the inverse of the assigned channel coefficient [Pro95]. The drawback of ZF equalization is that for small amplitudes of  $\underline{H}_l$  the equalizer enhances the noise  $\underline{N}_l$  in such a way that the SNR  $\gamma_c$  may go to zero on some subcarriers.

**Minimum Mean Square Error (MMSE) Equalization:** Equalization according to the MMSE criterion minimizes the mean square value of the error

$$\varepsilon_l = \underline{S}_l - \underline{G}_l \underline{R}_l \quad (3.61)$$

between the transmitted signal and the output of the equalizer. The mean square error

$$J_l = \text{E}\{|\varepsilon_l|^2\} \quad (3.62)$$

can be minimized by applying the orthogonality principle [Pap91, PrM96], stating that the mean square error  $J_l$  is minimum if the equalizer coefficient  $\underline{G}_l$  is selected such that the error  $\varepsilon_l$  is orthogonal to the received signal  $\underline{R}_l^*$ , i.e.,

$$\text{E}\{\varepsilon_l \underline{R}_l^*\} = 0. \quad (3.63)$$

With (3.48), (3.61), and (3.63), the equalization coefficients based on the MMSE criterion result in

$$\underline{G}_l = \frac{\underline{H}_l^*}{|\underline{H}_l|^2 + 1/\gamma_c}. \quad (3.64)$$

The computation of the MMSE equalization coefficients requires an estimation of the actual SNR per subcarrier  $\gamma_c$ , cf. Section 3.3.1. For  $\gamma_c \rightarrow \infty$ , the MMSE equalizer is identical to the ZF equalizer.

**Suboptimal MMSE Equalization:** To overcome the additional complexity due to the estimation of  $\gamma_c$  with MMSE equalization, a low-complex suboptimal MMSE equalization can be realized [Kai95b]. With suboptimal MMSE equalization, the equalization coefficients are designed such that they perform optimally only in the most critical case at which successful transmission should be guaranteed. In the other cases, the coefficients are suboptimal since the information about the actual  $\gamma_c$  is not used in the equalizer. Thus,  $K_q$  is set equal to the upper bound  $L$ , cf. (3.36), and  $\gamma_c$  becomes equal to  $\gamma_s$ , cf. (3.51). The SNR  $\gamma_s$  is set equal to a threshold  $\lambda$  at which the optimal MMSE equalization guarantees the maximum acceptable BER. The equalization coefficient with suboptimal MMSE equalization results in

$$G_l = \frac{H_l^*}{|H_l|^2 + \lambda} \quad (3.65)$$

and requires only information about  $H_l$ . The value  $\lambda$  has to be determined by investigations carried out in advance.

**Controlled Equalization:** Controlled equalization, also referred to as threshold ORC (TORC) or smooth ORC (SORC), applies ZF equalization to avoid MAI only on a subcarrier where the amplitude of the channel coefficient  $H_l$  exceeds a predefined threshold  $a_{\text{thresh}}$  [YeL94a]. A subcarrier with a small fading amplitude, which may be dominated by a noise component, is set to a certain value  $\xi_l$ , with the intention of preventing strong noise amplification. Thus, the equalization coefficient is defined as

$$G_l = \begin{cases} \frac{1}{H_l} & \text{if } |H_l| \geq a_{\text{thresh}} \\ \xi_l & \text{if } |H_l| < a_{\text{thresh}} \end{cases} . \quad (3.66)$$

In [YeL94a] it is proposed to neglect subcarriers with small amplitudes of the channel coefficients, yielding

$$\xi_l = 0. \quad (3.67)$$

An improvement is achievable when applying EGC on the strong faded subcarriers [Kai95b], so that the information on these subcarriers is not completely neglected, i.e.,

$$\xi_l = \frac{H_l^*}{|H_l|}. \quad (3.68)$$

A further improvement can be achieved by choosing

$$\xi_l = \frac{H_l^*}{|H_l| a_{\text{thresh}}} \quad (3.69)$$

as considered in [RoB96]. Common to all three variants of controlled equalization is that the threshold  $a_{\text{thresh}}$  depends on both the SNR  $\gamma_s$  and the number of active users  $K_q$  and that the optimum  $a_{\text{thresh}}$  has to be found by investigations carried out in advance.

### 3.3.3 Interference Cancellation

MD with IC is carried out iteratively in multiple detection stages. Values and functions related to the  $j$ th iteration are marked by an index  $[j]$ , where  $j$  may take on the values  $1, \dots, J_{\text{it}}$ , and  $J_{\text{it}}$  is the total number of iterations. The initial detection stage is indicated by the index  $[0]$ . A parallel IC realization is described in the sequel. Successive IC can easily be derived from parallel IC by only cancelling the contribution of the strongest interferer per detection stage.

In the initial detection stage, the data symbols of all  $K_q$  active users are detected in parallel by SD. That is,

$$\hat{\underline{d}}^{(k)[0]} = \mathbf{Q} \left\{ \underline{\mathbf{c}}^{(k)*} \underline{\mathbf{G}}^{[0]} \underline{\mathbf{r}}^{\text{T}} \right\}, \quad k = 1, \dots, K_q, \quad (3.70)$$

where  $\underline{\mathbf{G}}^{[0]}$  and  $\hat{\underline{d}}^{(k)[0]}$  denote the equalization coefficients and the detected data symbol of the  $k$ th user, respectively, assigned to the initial stage. The following detection stages work iteratively by using the decisions of the previous stage to reconstruct the interfering contribution in the received signal. The obtained interference is subtracted, i.e., cancelled from the received signal and the data detection is performed again with reduced MAI. Thus, the second and further detection stages apply

$$\hat{\underline{d}}^{(k)[j]} = \mathbf{Q} \left\{ \underline{\mathbf{c}}^{(k)*} \underline{\mathbf{G}}^{[j]} \left( \underline{\mathbf{r}} - \underline{\mathbf{H}} \sum_{\substack{g=1 \\ g \neq k}}^{K_q} \hat{\underline{d}}^{(g)[j-1]} \underline{\mathbf{c}}^{(g)} \right)^{\text{T}} \right\}, \quad j = 1, \dots, J_{\text{it}}, \quad (3.71)$$

where except for the final stage the detection according to (3.71) has to be applied for all  $K_q$  users.

The equalization matrix  $\underline{\mathbf{G}}^{[j]}$  should be adapted to the detection stages such that in the initial stage an SD technique is employed which can cope with MAI, where in the following stages an SD technique suitable for the quasi MAI-free case should be exploited. Therefore, the performance of an MC-CDMA system first introduced with IC using EGC in all stages [Faz93] is poor compared to IC with equalizers adapted to the detection stages [Kai95c, Kai95b]. Very promising results are obtained with MMSE equalization adapted to the  $K_q$  active users in the initial stage, followed by MMSE equalization adapted to the single user case in the previous detection stages [Kai95b].

The application of MRC seems theoretically to be of advantage for the second and further detection stages, since MRC is the best detection technique in the MAI-free, i.e., in the single user case. However, if one or more decision errors are made in one detection stage, MRC performs poorly even with only one wrong decision [Kai95c]. Hence, the average BER with MRC in the second and further stages cannot reach the performance of an MMSE equalizer adapted to the single user case with  $K_q$  equal to 1 in the second and further stages, since the latter is less sensitive to decision errors. Other combinations of SD in the different detection stages are proposed in [HLP95] with ZF equalization followed by MRC, and improved in [KaP96b] with controlled equalization followed by MRC. Since IC with adapted MMSE equalization outperforms the other concepts with respect to the BER, the realization of IC with suboptimal

MMSE equalizers adapted to the detection stages seems to be a good compromise between performance and complexity.

### 3.3.4 Joint Detection with Maximum Likelihood Criterion

The optimum detection technique exploits the maximum a posteriori (MAP) criterion or the maximum likelihood (ML) criterion, respectively, [Pro95] and is based on JD. In this section, two optimum ML detection algorithms are presented, namely the maximum likelihood sequence estimation (MLSE), which optimally estimates the transmitted data sequence  $\mathbf{d}$ , and the maximum likelihood symbol-by-symbol estimation (MLSSE), which optimally estimates the transmitted data symbol  $d^{(k)}$ . It is straightforward, that both algorithms can be extended to a MAP sequence estimator and to a MAP symbol-by-symbol estimator by taking into account the a priori probability of the transmitted sequence and symbol, respectively [Pro95]. However, since within this thesis all possible transmitted sequences and symbols, respectively, are assumed to be equally probable a priori, the estimator based on the MAP criterion and the one based on the ML criterion are equivalent [Pro95]. The possible transmitted data symbol vectors are  $\mathbf{d}_\mu$ ,  $\mu = 1, \dots, M_d^{K_q}$ , where  $M_d^{K_q}$  is the number of possible transmitted data symbol vectors.

The **MLSE** minimizes the sequence error probability, i.e., the data symbol vector error probability, which is equivalent to maximizing the conditional probability  $P\{\mathbf{d}_\mu|\mathbf{r}\}$  that  $\mathbf{d}_\mu$  was transmitted given  $\mathbf{r}$  according to (3.43). The estimate of  $\mathbf{d}$  obtained with MLSE is

$$\hat{\mathbf{d}} = \arg \max_{\mathbf{d}_\mu} P\{\mathbf{d}_\mu|\mathbf{r}\}, \quad (3.72)$$

with  $\arg$  denoting the argument of the function. By using Bayes' rule [Pap91], the conditional probability  $P\{\mathbf{d}_\mu|\mathbf{r}\}$  can be written as

$$P\{\mathbf{d}_\mu|\mathbf{r}\} = \frac{p(\mathbf{r}|\mathbf{d}_\mu)P\{\mathbf{d}_\mu\}}{p(\mathbf{r})}, \quad \mu = 1, \dots, M_d^{K_q}. \quad (3.73)$$

When assuming that all vectors  $\mathbf{d}_\mu$ ,  $\mu = 1, \dots, M_d^{K_q}$ , are equally probable and by noting that the denominator in (3.73) is independent of the transmitted data symbol vector, the decision rule based on finding the sequence that maximizes  $P\{\mathbf{d}_\mu|\mathbf{r}\}$  is equivalent to finding the sequence that maximizes  $p(\mathbf{r}|\mathbf{d}_\mu)$ . The conditional probability density function  $p(\mathbf{r}|\mathbf{d}_\mu)$  of the received vector  $\mathbf{r}$  given  $\mathbf{d}_\mu$  is referred to as a likelihood function. With independent noise on the subcarriers, the received values  $R_l$ ,  $l = 1, \dots, L$ , cf. (3.43) and (3.12), are statistically independent and  $p(\mathbf{r}|\mathbf{d}_\mu)$  may be expressed as [Pap91]

$$p(\mathbf{r}|\mathbf{d}_\mu) = \prod_{l=1}^L p(R_l|\mathbf{d}_\mu), \quad \mu = 1, \dots, M_d^{K_q}. \quad (3.74)$$

With complex-valued AWGN on the subcarriers,  $p(R_l|\mathbf{d}_\mu)$  is given by [Pro95]

$$p(R_l|\mathbf{d}_\mu) = \frac{1}{\pi\sigma^2} \exp\left(-\frac{1}{\sigma^2} |R_l - H_l \mathbf{c}_l \mathbf{d}_\mu^\Gamma|^2\right), \quad \mu = 1, \dots, M_d^{K_q}, \quad (3.75)$$

where  $\underline{\mathbf{c}}_l$  is the  $l$ th row of the spreading code matrix  $\mathbf{C}$  defined in (3.45). Substitution of (3.75) into (3.74) leads to the likelihood function

$$p(\mathbf{r}|\underline{\mathbf{d}}_\mu) = \left(\frac{1}{\pi\sigma^2}\right)^L \exp\left(-\frac{1}{\sigma^2} \|\mathbf{r} - \mathbf{H}\mathbf{C}\underline{\mathbf{d}}_\mu\|^2\right), \quad \mu = 1, \dots, M_d^{K_q}. \quad (3.76)$$

Since the reciprocal exponential function is a monotonously decreasing function, the maximum of  $p(\mathbf{r}|\underline{\mathbf{d}}_\mu)$  over  $\underline{\mathbf{d}}_\mu$  is equivalent to finding the data symbol vector  $\underline{\mathbf{d}}_\mu$  that minimizes the squared Euclidean distance

$$\Delta^2(\underline{\mathbf{d}}_\mu, \mathbf{r}) = \|\mathbf{r} - \mathbf{H}\mathbf{C}\underline{\mathbf{d}}_\mu\|^2, \quad \mu = 1, \dots, M_d^{K_q}, \quad (3.77)$$

between the received and all possible transmitted sequences. The most likely transmitted data vector can be expressed as [Pro95, FaP93]

$$\hat{\underline{\mathbf{d}}} = \arg \min_{\underline{\mathbf{d}}_\mu} \Delta^2(\underline{\mathbf{d}}_\mu, \mathbf{r}). \quad (3.78)$$

Thus, the MLSE requires the evaluation of  $M_d^{K_q}$  squared Euclidean distances per estimation step.

The **MLSSE** minimizes the symbol error probability, which is equivalent to maximizing the conditional probability  $P\{\underline{\mathbf{d}}_\mu^{(k)}|\mathbf{r}\}$  that  $\underline{\mathbf{d}}_\mu^{(k)}$  was transmitted given  $\mathbf{r}$ . The estimate of  $\underline{\mathbf{d}}^{(k)}$  obtained by MLSSE is

$$\hat{\underline{\mathbf{d}}}^{(k)} = \arg \max_{\underline{\mathbf{d}}_\mu^{(k)}} P\{\underline{\mathbf{d}}_\mu^{(k)}|\mathbf{r}\}. \quad (3.79)$$

The conditional probability  $P\{\underline{\mathbf{d}}_\mu^{(k)}|\mathbf{r}\}$  is given by

$$P\{\underline{\mathbf{d}}_\mu^{(k)}|\mathbf{r}\} = \sum_{\substack{\forall \underline{\mathbf{d}}_\mu \text{ with same} \\ \text{realization of } \underline{\mathbf{d}}_\mu^{(k)}}} P\{\underline{\mathbf{d}}_\mu|\mathbf{r}\}, \quad \mu = 1, \dots, M_d^{K_q}, \quad (3.80)$$

where the probability  $P\{\underline{\mathbf{d}}_\mu^{(k)}|\mathbf{r}\}$  is the union of all mutually exclusive events  $P\{\underline{\mathbf{d}}_\mu|\mathbf{r}\}$  with the same realization of  $\underline{\mathbf{d}}_\mu^{(k)}$  [Pap91, KaP96a]. By using Bayes' rule and assuming that all data symbols  $\underline{\mathbf{d}}_\mu^{(k)}$  are equally probable and by noting that  $p(\mathbf{r})$  is independent of the transmitted data symbol, the decision rule based on finding the symbol that maximizes  $P\{\underline{\mathbf{d}}_\mu^{(k)}|\mathbf{r}\}$  is equivalent to finding the symbol that maximizes  $p(\mathbf{r}|\underline{\mathbf{d}}_\mu^{(k)})$ . Thus, with (3.79), (3.80), and (3.76), by ignoring the constant factor  $1/(\pi\sigma^2)^L$  which is independent of the transmitted data symbol, the most likely transmitted data symbol is

$$\hat{\underline{\mathbf{d}}}^{(k)} = \arg \max_{\underline{\mathbf{d}}_\mu^{(k)}} \sum_{\substack{\forall \underline{\mathbf{d}}_\mu \text{ with same} \\ \text{realization of } \underline{\mathbf{d}}_\mu^{(k)}}} \exp\left(-\frac{1}{\sigma^2} \Delta^2(\underline{\mathbf{d}}_\mu, \mathbf{r})\right). \quad (3.81)$$

The increased complexity with MLSSE compared to MLSE can be observed in the comparison of (3.81) with (3.78), where besides the evaluation of the  $M_d^{K_q}$  squared Euclidean distances, the sum over the exponential functions of the squared Euclidean distances for all realizations

of  $\underline{d}_\mu^{(k)}$  has to be calculated. Furthermore, knowledge about the variance of the noise  $\sigma^2$  is required with MLSSE compared to MLSE. Both JD techniques require knowledge about which user is active, i.e., which user specific spreading code is actually in use. An advantage of MLSSE compared to MLSE is that the MLSSE inherently generates a reliability information for a detected data symbols  $\hat{\underline{d}}^{(k)}$  which can be exploited in a subsequent soft decision channel decoder, cf. Chapter 4. Since the MLSSE is the optimal symbol detector, the MLSSE reaches a lower symbol error rate compared to the MLSE. However, the improvements with MLSSE are small and often do not justify its additional complexity.

It should be noted that there exist also suboptimal JD techniques for MC-CDMA systems [JBP96b]. Generally, CDMA systems which have to cope with ISI in the detection process are in practice not able to exploit optimum JD with MLSE or MLSSE and require suboptimal approaches [Kle96]. However, due to the avoidance of ISI in the detection process and by employing the  $Q$ -Modification in the presented MC-CDMA system, it is possible to implement the optimum JD techniques with reasonable complexity in MC-CDMA systems [FaP93].

### 3.4 Performance of Uncoded MC-CDMA Systems

In this section, the performance of different MC-CDMA data detection techniques is shown and compared to each other for the downlink. To evaluate the performance, an MC-CDMA reference system is defined in the following. Since the investigations should focus on the performance of the data detection techniques, the MC-CDMA reference system is defined without channel coding and assumes perfect channel estimation. The used spreading codes are orthogonal Walsh-Hadamard codes [Pro95] with the purpose to minimize the MAI. The spreading code length in a subsystem is  $L$  equal to 8, which is motivated by the results presented in [Kai96], cf. Section 4.6, and in [ScK96]. Thus, each subsystem can maximally handle  $K_{q,\max}$  equal to 8 users. Unless otherwise stated, the case with fully loaded subsystem is considered in the sequel. QPSK with Gray encoding is applied for data symbol mapping [Pro95]. Moreover, the guard interval of the reference system is chosen such that ISI and ICI are completely eliminated. By assuming one of the three modified MC-CDMA systems presented in Figs. 3.8, 3.9, and 3.10, the channel fading on the subcarriers per subsystem is modelled by uncorrelated flat fading due to frequency interleaving. The mobile radio channel is implemented as uncorrelated Rayleigh fading channel, described in detail in Section 2.2.2. Table 3.1 briefly summarizes the parameters of the MC-CDMA reference system used in this section. The performance of the MC-CDMA reference system presented in this section is applicable to any MC-CDMA system with an arbitrary transmission bandwidth  $B$ , an arbitrary number of subsystems  $Q$ , and an arbitrary number of data symbols  $M$  transmitted per user in an OFDM symbol. Only the number of subcarriers within a subsystem has to be 8 and the amplitudes of the channel fading have to be Rayleigh distributed and can be considered as uncorrelated on the subcarriers of a subsystem due to appropriate frequency interleaving. The loss in SNR  $V_{\text{guard}}$  due to the guard interval, cf. (3.23), is not taken into account in the results presented for the MC-CDMA reference system

Table 3.1: Parameters of the MC-CDMA reference system

spreading code	Walsh-Hadamard code
spreading code length	$L = 8$
maximum number of users per subsystem	$K_{q,\max} = 8$
data symbol mapping	QPSK with Gray encoding
channel coding	no
channel estimation	perfect
channel	uncorrelated Rayleigh fading channel

in Chapters 3 and 4. The intention is that the loss in SNR due to the guard interval can be calculated according to (3.23) individually for each specified guard interval. So, the presented results can generally be modified for any guard interval. Moreover, in contrast to the results presented in Chapter 6, the results presented in Chapters 3 and 4 do not take into account an SNR loss due to the transmission of pilot symbols required for channel estimation.

As reference for the evaluation of the different SD and MD techniques, the MF bound of an MC-CDMA system is used as a lower bound. The MF bound of an uncoded MC-CDMA system with uncorrelated Rayleigh fading on the subcarriers corresponds to the BER  $P_b$  obtained from data transmission over  $L$  statistically independent Rayleigh fading channels combined with MRC [Pro95], given by

$$P_b = \left( \frac{1}{2} - \frac{1}{2} \sqrt{\frac{\gamma_b}{L + \gamma_b}} \right)^L \sum_{l=0}^{L-1} \binom{L-1+l}{l} \left( \frac{1}{2} + \frac{1}{2} \sqrt{\frac{\gamma_b}{L + \gamma_b}} \right)^l, \quad (3.82)$$

where  $\gamma_b$  is the SNR per bit defined according to (3.52) and  $L$  is the spreading code length. If the fading is correlated between the subcarriers of a subsystem and the diversity  $D$  offered by the channel is smaller than the spreading code length  $L$ , by still having Rayleigh distributed fading amplitudes, (3.82) remains a lower bound. The MF bound of uncoded MC-FDMA and MC-TDMA systems, in the following referred to as the MC-FDMA/MC-TDMA MF bound, is obtained from (3.82) by choosing  $L$  equal to 1, since these systems achieve no diversity gain without channel coding.

The theoretically calculated MF bounds of MC-CDMA systems with different spreading code lengths  $L$  and for MC-FDMA and MC-TDMA systems in an uncorrelated Rayleigh fading channel are depicted in Fig. 3.14. The MF bounds for the MC-CDMA reference system with  $L$  equal to 8 and for MC-FDMA and MC-TDMA systems in an uncorrelated Rayleigh fading channel are included as reference in the following BER curves presented in this section. Furthermore, the performance of the MC-CDMA, MC-FDMA, and MC-TDMA systems in an AWGN channel, also referred to as ideal channel, is illustrated. The performance of the various systems in the AWGN channel is due to the absence of MAI identical and can be calculated

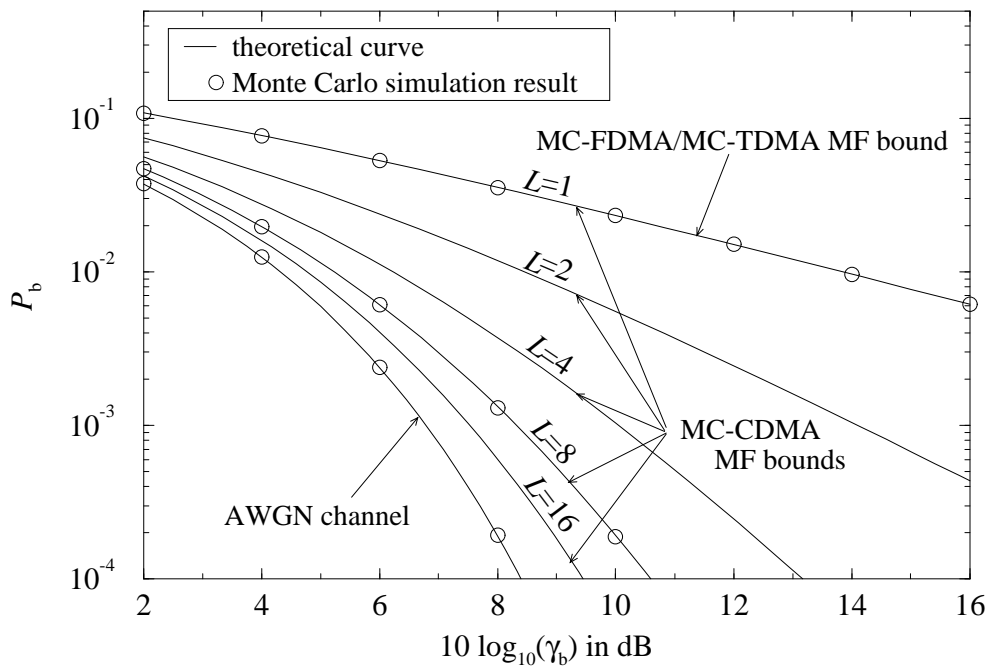


Figure 3.14: MF bounds for uncoded MC-CDMA systems with different spreading code lengths and of MC-FDMA and MC-TDMA systems; uncorrelated Rayleigh fading channel and AWGN channel; QPSK

according to [Pro95]

$$P_b = \frac{1}{2} \operatorname{erfc}(\sqrt{\gamma_b}). \quad (3.83)$$

The theoretical results of the MC-CDMA reference system, of MC-FDMA and MC-TDMA systems for the uncorrelated Rayleigh fading channel and the AWGN channel in Fig. 3.14 are confirmed by Monte Carlo simulation results. The performance curves presented in the following are obtained by Monte Carlo simulations if nothing different is explicitly stated. Since, for instance, in the case of speech transmission an uncoded BER  $P_b$  of about  $10^{-2}$  is required which leads to a BER  $P_b$  of about  $10^{-3}$  at the output of the channel decoder, the uncoded BER  $P_b$  equal to  $10^{-2}$  is focused on in the following considerations.

The average uncoded BER  $P_b$  versus the SNR  $\gamma_b$  per bit for the SD techniques MRC, EGC, ZF equalization, and MMSE equalization applied in the MC-CDMA reference system is depicted in Fig. 3.15. The results show that with a fully loaded subsystem the MMSE equalization outperforms the other investigated SD techniques. ZF equalization restores the orthogonality between the user signals and avoids MAI, however, it introduces noise amplification which is especially high at low SNRs. EGC avoids noise amplification but does not counteract the MAI caused by the loss of the orthogonality between the user signals, resulting in a high error floor. The worst performance is obtained with MRC which additionally enhances the MAI, cf. Section 3.3.2. The error floor with MRC and with EGC can be analytically evaluated [YLF93, YeL94a, Kai95c].

In Fig. 3.16, the average uncoded BER  $P_b$  versus the SNR  $\gamma_b$  per bit for the SD techniques

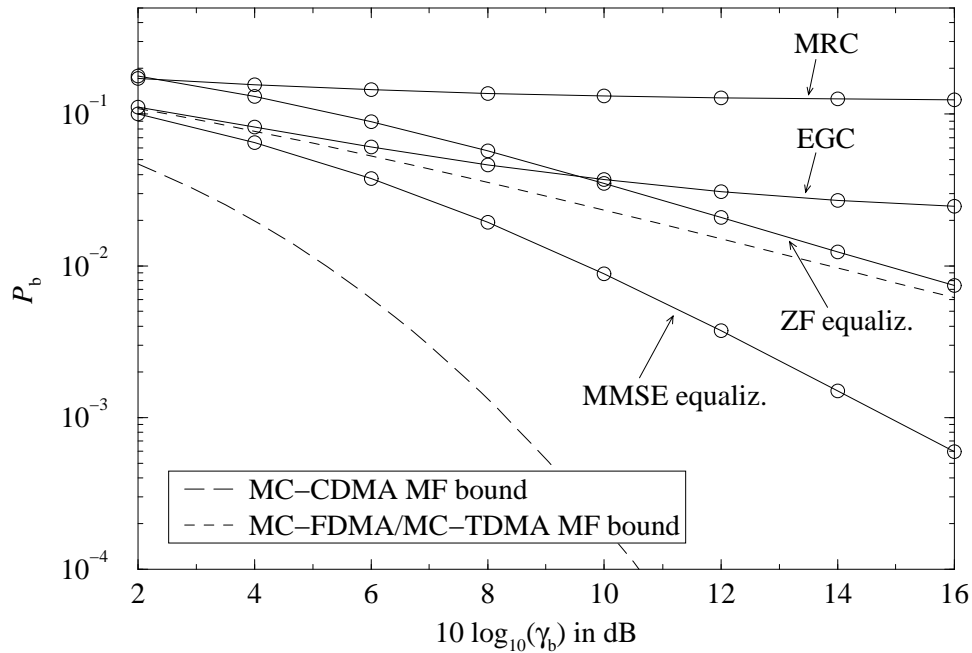


Figure 3.15: Average uncoded BER  $P_b$  versus SNR  $\gamma_b$  for SD with MRC, EGC, ZF equalization, and MMSE equalization; uncorrelated Rayleigh fading channel;  $L = 8$ ;  $K_q = 8$ ; QPSK

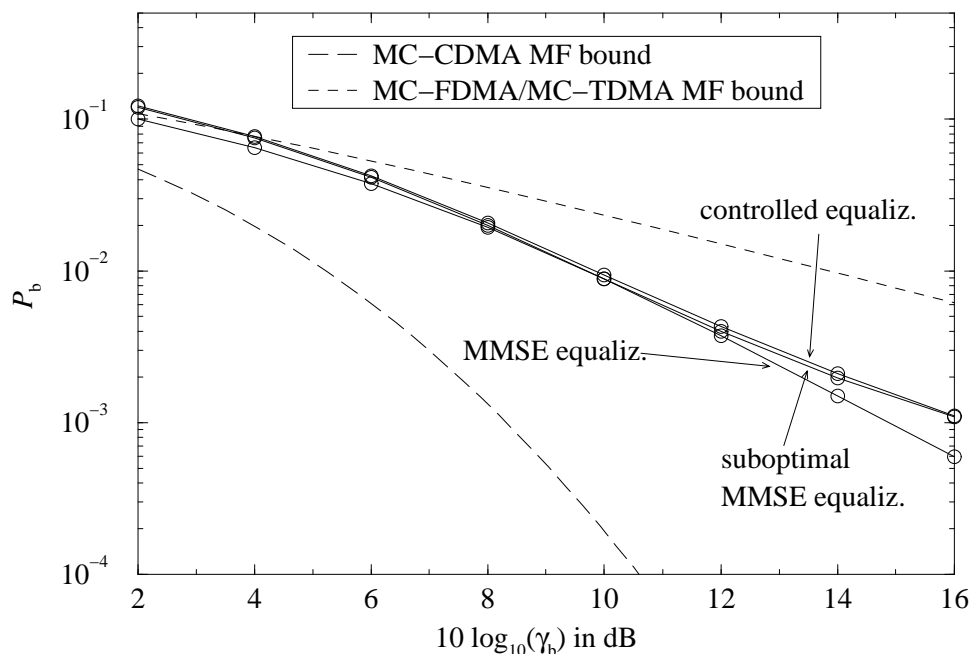


Figure 3.16: Average uncoded BER  $P_b$  versus SNR  $\gamma_b$  for SD with MMSE equalization, suboptimal MMSE equalization, and controlled equalization; uncorrelated Rayleigh fading channel;  $L = 8$ ;  $K_q = 8$ ; QPSK





















































































































































































































































































































































































































